Title

Early rhombic lip Protogenin+ve stem cells in a human-specific neurovascular niche initiate and maintain group 3 medulloblastoma.

Journal

Cell, 187(17)

Authors

Visvanathan, Abhirami
Saulnier, Olivier
Chen, Chuan
et al.

Publication Date

2024-08-22

DOI

10.1016/j.cell.2024.06.011

Peer reviewed

HHS Public Access

Author manuscript

Cell. Author manuscript; available in PMC 2025 January 08.

Published in final edited form as:

Cell. 2024 August 22; 187(17): 4733–4750.e26. doi:10.1016/j.cell.2024.06.011.

Early Rhombic Lip Protogenin^{+ve} Stem Cells in a Human Specific Neurovascular Niche Initiate and Maintain Group 3 Medulloblastoma

A full list of authors and affiliations appears at the end of the article.

Summary

We identify a population of PRTG^{+ve} MYC^{high} NESTIN^{low} stem cells in the four-week-old human embryonic hindbrain that subsequently localizes to the ventricular zone of the rhombic lip (RL^{VZ}). Oncogenic transformation of early Prtg^{+ve} rhombic lip stem cells initiate Group 3 Medulloblastoma (Gr3-MB)-like tumors. PRTG^{+ve} stem-cells grow adjacent to a human specific interposed vascular plexus in the RL^{VZ}, a phenotype which is recapitulated in Gr3-MB, but not other types of medulloblastoma. Co-culture of Gr3-MB with endothelial cells promotes tumor stem-cell growth, with the endothelial cells adopting an immature phenotype. Targeting the PRTG^{high} compartment of Gr3-MB *in vivo* using either the diphtheria toxin system, or chimeric antigen receptor T-cells constitutes effective therapy. Human Gr3-MBs likely arise from early embryonic RL^{VZ} PRTG^{+ve} stem cells inhabiting a specific perivascular niche. Targeting either the PRTG^{high} compartment, and/or the perivascular niche represents an approach to treat children with Gr3-MB.

Keywords

Rhombic lip; cancer genomics; perivascular niche; Group 3 medulloblastoma; brain tumor immunotherapy

Introduction

‘Medulloblastomas’ are the most common malignant brain tumors of childhood and arise in the embryonal hindbrain of humans. Molecular stratification delineates four

Lead Contact: mdt.cns@gmail.com.

†These authors contributed equally to this work

*These authors jointly supervised this work

Author contributions

AV, OSa and CC designed, performed, and analyzed most of the experiments in this study. PH. contributed to in situ hybridization and interpretation. WO and AD contributed to staining of medulloblastoma patient samples. WL provided peptide library. JM and JG contributed to in-situ hybridization. WOn and MCV contributed to single-cell preparation. AR contributed to SCENIC workflow. TN and YF contributed to tissue data collection. LDH contributed to scRNA seq analysis. BL., NA., and VF contributed to imaging. JYL, CR and JH contributed to *in vivo* experiments. VP contributed to RNA-seq analysis. SS, XuW, RVO, ML, KK, PB, AE, JZ, MKS and OS contributed to experiments. ZB and AB contributed to human CS12 analysis. RS, HW, NH, JP and TD contributed to *in vivo* experiments. FR, and ES, provided human samples. KAA, AKM, LG, CLK, LDS, PD, RWR, NJ, WW, JR., HS, DS, DE and KJM provided expert advice. XW and CD provided reagents and expert advice. DSD, and MDT jointly supervised the project. AV, OSa, CC and MDT prepared the figures and wrote the manuscript.

Competing interests

The authors declare no competing interests. Patent submitted by University of Pittsburgh (University Docket No. 05700 / F&R Ref 48881-0028P01). US 63/275,326 Molecules that bind to Protogenin polypeptides.

transcriptional subgroups of medulloblastoma: SHH, WNT, Group 3 (Gr3-MB) and Group 4 (Gr4-MB). Gr3-MB is associated with poor survival, and frequent metastases at diagnosis[1,2]. The cellular and molecular mechanisms underlying Gr3-MB tumorigenesis are not well understood.

Human brain development, including the spatial compartmentalization of the rhombic lip (RL), is markedly distinct from other mammals[3,4]. We identify first trimester Protogenin (PRTG)^{high} stem-like cells in the hindbrain neural plate and subsequent RL ventricular zone (RL^{VZ}) as the apex of the Gr3-MB cellular hierarchy. PRTG is a membrane protein known to prevent precocious differentiation, and apoptosis during early neural tube development[5]. PRTG^{+ve} cells in both normal human RL^{VZ} and Gr3-MB grow adjacent to a CD34^{+ve} immature vascular plexus, suggesting the existence of a perivascular niche supporting stem cell maintenance. Defects of the RL^{VZ} interposed vascular plexus (IVP) are associated with severe cerebellar hypoplasia[6]. Conversely, our results suggest a model in which Gr3-MB apical stem cells maintain a persistent, immature symbiotic neurovascular niche, with an endothelium transcriptionally similar to the RL^{VZ} IVP.

The goal of identifying cancer stem cells was driven by the hypothesis that ablation of this minority/apical population would have a therapeutic effect on the entire tumor. Indeed, targeting the PRTG^{high} compartment using anti-PRTG blocking antibodies, diphtheria-toxin mediated ablation, or anti-PRTG chimeric antigen receptor T-cells (CAR T-cells), demonstrates promising efficacy against Gr3-MB *in vivo* in pre-clinical models. Our data support a model in which PRTG^{+ve}/SOX2^{+ve}/MYC^{high}/NESTIN^{low} stem cells initiate and sustain Gr3-MB in an immature perivascular niche, and that ablation of cells in this compartment using immunotherapy is a successful therapeutic approach to treat Gr3-MB.

Results

Apical Gr3-MB RL^{VZ}-like stem cells mirror *CS12* hindbrain transcriptomes.

To identify the cells at the apex of the Gr3-MB hierarchy, we performed single-cell RNA sequencing (scRNA-seq) on six Gr3-MB patient tumors and were able to discern nine distinct transcriptional signatures (Figure. 1A, S1A, Table S1) without sample bias (Figure.S1B). Tumor cells were identified through expression of known Gr3-MB oncogenes such as *MYC* and *OTX2*, and the presence of copy number aberrations (Figure.S1A, C). Three distinct clusters of Gr3-MB cells were observed, and agnostically labelled as Gr3-A, Gr3-B and Gr3-C (Figure.S1A). Gr3-A was enriched for genes expressed in differentiated glutamatergic neurons, while Gr3-B was enriched for actively cycling cells expressing stem-like markers (Figure.S1A).

The phenotypes identified to date in pediatric cancers are largely retained, rather than acquired, due to unresolved fetal transcriptional states. To understand the hierarchy of Gr3-MB, we examined the lineage hierarchy in the normal human embryonic hindbrain at Carnegie Stage 12 (CS12 – 30 days post fertilization). Embryonic hindbrain cells resolved into four transcriptionally distinct clusters: NSCs, neuronal progenitors, migrating neural crest cells (mNCCs) and erythrocytes (Figure. 1B and Table S2). Trajectory inference demonstrated a hierarchical lineage with *PRTG*$^{+ve}$/*SOX2*$^{+ve}$ stem cells at the

apex, (Figure.1C, D) as well as differentiated progenitors (*NEUROD1*$^{+ve}$/*STMN2*$^{+ve}$) [7], and mNCCs expressing pre-EMT markers (*TWIST1*^{high}/*MSX1*^{high})[8] (Figure.1D). Cerebellar neurons originate from two germinal zones, the *V*entricular *Z*one and the Rhombic Lip[9]. The RL is a thickening of the neural tube, located at the dorsal end of the 4th ventricle. The *Homo sapiens* RL exhibits a unique spatiotemporal split around 10-11 post conception weeks (PCW) into a ventricular zone (RL^{VZ}) containing SOX2^{+ve} stem cells, and a subventricular zone (RL^{SVZ}) with high Ki67^{+ve} progenitor cells[3] (Figure.1E). Interposed between the RL^{VZ} and the RL^{SVZ} was a *Homo sapiens* specific GFAP^{+ve}/CD34^{+ve} interposed vascular plexus (IVP) (Figure. 1E). In the CS19 human hindbrain, PRTG expression was limited to the RL (Figure.1F). Post RL split, these cells localized to the RL^{VZ} at 17PCW, exhibited high *MYC* expression, and were juxtaposed to the GFAP^{+ve}/CD34^{+ve} IVP (Figure.1E, F)

Expression and transcriptional activity of MYC was compartmentalized to the RL^{VZ} (Figure. 1F, S1E, F). High PRTG expression in the early RL^{VZ}, and absence in the downstream glutamatergic neuronal hierarchy was confirmed from PCW9 to PCW20 (Figure. 1G). PRTG^{high} /MYC^{high} compartment cells lack *NESTIN* expression (Figure.S1G). We conclude that the RL^{VZ} apical stem-like population expresses *PRTG*, *SOX2*, and *MYC* during early hindbrain development. Transcriptional profiling of flow-sorted PRTG^{high} versus PRTG^{low} cells from Gr3-MB xenografts demonstrates high activity of oncogenic transcription factors in the PRTG^{high} compartment, with more differentiated neuronal markers (*LHX2* and *NEUROD1*) in the PRTG^{low} compartment (Figure.S1H).

Despite the murine RL lacking either conspicuous compartmentalization, or the rhombic lip IVP (RL-IVP) vasculature observed in *Homo sapiens*, it does demonstrate some dorsal-ventral compartmentalization of unipolar brush cells (UBCs– *Lmx1a* expression), and granule cell progenitors (GCPs– *Atoh1*expression)[10]. Indeed, Prtg expression was biased to the ventral aspect of the E9.5 RL in Prtg^{eGFP} mice, but largely extinguished by E10.5 (Figure S2A, B). Expression of Nestin (NSC), Lmx1a (UBC progenitor) and Pax6 (RL glutamatergic derivatives)[11] were mutually exclusive with Prtg in the E10 RL (Figure.S2C). Conversely, Atoh1, an early marker of the RL-derived glutamatergic progenitors overlaps with a few Prtg^{+ve} cells, suggesting that the latter were committed to the glutamatergic lineage (Figure.S2C). Concordantly, PRTG^{+ve} cells in Gr3-MB showed co-expression of *ATOH1* and *SOX2*, but not *PAX6* or *NESTIN*, or *LMX1A* (Figure.S2D).

Comparison of Gr3-MB scRNA-seq clusters to the human CS12 hindbrain demonstrated most Gr3-MB cells belong to the neuronal progenitor lineage (Figure.1H). However, a minor subset mirrors the early NSC cluster, including expression of *PRTG* and *SOX2* (Figure.1I). Unlike Gr3-MB, Gr4-MB tumor cells lack the NSC-like cluster, suggesting that Gr4-MBs initiate later in the differentiation trajectory than CS12 (Figure.1I). PRTG, a transmembrane protein known to inhibit neuronal differentiation[5] marks the normal CS12 NSC cluster (Figure.1J). PRTG was most highly expressed in Gr3γ tumors, the subtype with frequent *MYC* amplification, high metastases, and a poor prognosis[2] (Figure. 1K). These data suggest that *PRTG*$^{+ve}$/*SOX2*$^{+ve}$/*MYC*^{high}/*NESTIN*^{low} cells from the CS12 hindbrain are a putative cell of origin for Gr3-MB (Figure.1L).

Tumor initiating cell (TIC) compartment of Gr3-MB

To test the hypothesis that PRTG^{+ve} RL stem cells constitute the cell/lineage of origin for Gr3-MB, we isolated eGFP^{+ve} cells from the RL of E9.5 Prtg^{eGFP} mice and transformed them through expression of inducible *MycT58A* (an oncogenic allele of *Myc*), and/or silencing of *Tp53*. Transformation was assessed through anchorage independent growth. Transformed Prtg^{+ve} cells from E9.5 form frequent colonies, which were not observed in Prtg^{-ve} cells (Figure.2A, B). The ability to transform E9.5 Prtg^{+ve} cells was diminished by E11. Colonies from E9.5 transformed Prtg^{+ve} cells are larger than controls (Figure.2B).

Elevated *MYC* expression is a well-known somatic driver in Gr3-MB[12]. Hyper-transcription of *GFI1* and *GFI1B* through enhancer hijacking are also observed in Gr3-MB as well as Gr4-MB[13]. Mutation of the *hTERT* promoter is common in SHH-MB, but rare in Gr3-MB[14]. The well-known tumor suppressor gene locus, *P19^{Arf}*,[15] is inactivated in many human cancers, but infrequently inactivated in medulloblastoma. To formally test their transformability, we isolated RL Prtg^{+ve} cells from the hindbrain of E9.5 Prtg^{eGFP} or Prtg-cre mice and transformed with the following combinations: *MycT58A/shTp53 or LSL-MYC/Tp53DN*, *LSL-MYC/GFI1* (known Gr3-MB driver genes), versus *mTert/shP19^{Arf}* shRNA negative controls, and injected the modified cells into the cerebellum of NSG mice. Tumors formed in 3/11 *MycT58A/shTp53*, 4/7 *LSL-MYC/Tp53DN*, but 0/7 *mTert/shP19^{Arf}* mice (Figure. 2C, D). *LSL-Myc/TP53DN* tumors showed poor survival (Figure.2E) and were histologically similar to Gr3-MB with pleomorphic cells with polyhedral nuclei typical of a large-cell/anaplastic MB (Figure.2F). *LSL-Myc/TP53DN* tumors also retained a perivascular niche encompassing the Prtg^{+ve} cells similar to the fetal RL^{VZ} (Figure. S3A) and can form tumors in secondary recipient mice (Figure.S3B). *LSL-Myc/TP53DN* tumors express the Gr3-MB marker Npr3[16], and the stem cell marker Sox2 (Figure. S3C, D). Comparison of the transcriptional profile of Prtg^{+ve} stem cell derived mouse medulloblastomas to human medulloblastomas demonstrated similarity to human Gr3-MB (Figure. S3E). We conclude that the Prtg^{+ve} compartment of the early RL^{VZ} can be transformed to form embryonal tumors that histologically and transcriptionally resemble the large-cell/anaplastic variant of Gr3-MB, supporting a model in which PRTG^{+ve} stem cells from first trimester human hindbrain development are the cell/lineage of origin for Gr3-MB.

We detected PRTG on the cell surface (Figure.S3F), and in the cytoplasm of Gr3-MB (Figure.S3F). In the normal developing mouse brain, expression was limited to early time points (E9.5-E15.5) and diminished by P2 (Figure.S4A). A minority of Gr3-MB patient derived xenografts (PDX) cells express PRTG (Figure.S4B). We flow-sorted Gr3-MB PDXs into PRTG^{+ve} and PRTG^{-ve} fractions and undertook limited dilution analyses both *in vitro* (Figure. 2G) and *in vivo* (Figure. 2H, I). Across two different Gr3-MB PDXs, fewer PRTG^{+ve} cells were sufficient for tumorigenesis than PRTG^{-ve} cells both *in vitro*, and *in vivo* (Figure. 2G–I). The proteome varies greatly between the PRTG^{+ve} versus the PRTG^{-ve} compartments (Figure.S4C). PRTG^{+ve} cells exhibit high matrisome content (extracellular matrix associated and secreted proteins), validating their perivascular niche association (Figure.S4D). As PRTG is a known inhibitor of neuronal differentiation[5], we tested its function, rather than merely considering it as a cell surface marker. Diminished expression

of PRTG transcriptionally disrupts numerous neuronal developmental, synaptic plasticity and oncogenic pathways while inducing cell death related pathways (Figure. S4E–G, Table S3–5). The PRTG^{+ve} compartment of Gr3-MB transplants the tumor, and PRTG knockdown diminishes cellular fitness, suggesting that PRTG marks the tumor initiating compartment for Gr3-MB. PRTG protein blocking therapeutics might therefore provide an ideal route to targeting the apical compartment of Gr3-MB.

PRTG^{+ve} stem cells inhabit a perivascular niche in the RL^{VZ}

We agnostically compared the endothelial cells (ECs) from Gr3-MB, Gr4-MB, and SHH-MB from our scRNA-seq dataset using unsupervised clustering and found that ECs have subgroup specific recurrent transcriptional differences (Figure.3A). CD34 is an adhesion molecule expressed in hematopoietic progenitors and embryonal ECs[17]. During normal human hindbrain development at CS19 and 11PCW, the RL^{VZ} PRTG^{+ve} cells decorate the RL-IVP which contains both CD34^{+ve} and GFAP^{+ve} cells, interposed between the RL^{VZ} and RL^{SVZ} (Figure. 3B). Intriguingly, CD34 expression was restricted to the ECs of Gr3-MBs, but not Gr4-MBs or SHH-MBs (Figure. 3C). To further test whether Gr3-MBs mimic the fetal RL vasculature, we examined the spatial expression of additional Gr3-MB specific EC marker genes during hindbrain development. Expression of *ENG*, an angiogenic co-receptor of the Transforming Growth Factor-β trans-membrane complex[18], was enriched in the RL^{VZ} and adjacent fourth ventricular choroid plexus (4V-CP) at 11 and 18PCW (Figure.3D). *PLVAP*, an angiogenic fenestrated EC marker[19], was restricted to the early RL at CS19, and later to the 4V-CP, (Figure. 3E) as well as in the Gr3-MB endothelium (Figure.3E). *SERPINH1* and *IGFBP7* exhibit specific expression in the RL^{VZ} and adjacent CP, while *VWF* was restricted to the CP (Figure. S5A–C). *SPARC* and *COL4A1* were abundant in RL, CP and mesenchyme (Figure.S5D–F). *CD34, SERPINH1* and *COL4A1* were spatially confined to the RL, with expression in the RL-IVP at later developmental stages. Additionally, *OTX2*, a Gr3-MB oncogene secreted by the CP[20] was highly expressed in the adjacent RL (Figure.3F). The Gr4-MB specific oncogene *PRDM6* was detected in the 4V-CP at 17PCW. (Figure.3F).

Gr3-MB EC markers were also specifically expressed in the 4V-CP in addition to the RL-IVP. As the 4V-CP is directly juxtaposed to the rhombic lip/cerebellar nodulus during development, secreted factors from the 4V-CP likely affect rhombic lip development[21]. Intriguingly, portions of the 4V-CP arise directly from the RL primordium[22]. These data suggest a model in which the RL-IVP, and the adjacent 4V-CP secrete factors to support the growth and persistence of the sandwiched PRTG^{+ve} RL^{VZ} stem cells.

To validate the spatial distribution of PRTG^{+ve} cells in Gr3-MBs, we undertook immunohistochemical staining for PRTG protein across human embryonal tumors. PRTG protein expression was absent in surgical biopsies of Embryonal Tumors with Multi-layered Rosettes (ETMRs), or Atypical Teratoid/Rhabdoid Tumors (AT/RTs), SHH-MB or WNT-MB (Figure. 3G). However, luxuriant staining of PRTG^{+ve} clusters were observed in 10/15 Gr3-MB (Figure. 3H). Most Gr4-MB tumors were devoid of PRTG^{+ve} cells, while a few cases (7/36) showed sparse positive cells (Figure. 3G, H). The strong staining of

large numbers of clustered PRTG^{+ve} cells in Gr3-MB clearly contrasts with the individual scattered PRTG^{+ve} cells in a minority of Gr4-MB.

PRTG^{+ve} cells in Gr3-MBs were found in clusters, and were surrounded by abundant tumor vasculature, which was not observed in Gr4-MBs (Figure. 3H). Dual immunostaining of Gr3-MB patient tissue demonstrates PRTG^{+ve} clusters, surrounded by abnormal CD34^{+ve} cells, a relationship which is reminiscent of the normal RL^{VZ} PRTG^{+ve} cells and the RL-IVP (Figure.3I). Persistent Rhombic Lips (PeRLs) are observed after birth in the cerebellar nodulus, when the rhombic lip fails to complete its normal involution around the time of birth[6,23]. PeRLs often contain aberrant blood vessels, surrounded by a concentric arrangement of immature RL stem cells and progenitor cells, suggesting that the perivascular niche helps prevent differentiation. PeRLs are hypothesized to be the origin of MBs[24,25] (Figure.3J). Finally, leptomeningeal metastases of medulloblastoma frequently cluster around blood vessels. (Figure.3K). These data are consistent with a model in which both physiological and transformed RL^{VZ} stem cells thrive next to an immature vasculature, with the niche symbiotically promoting the inappropriate persistence of both cell types. Approaches to deprive the PRTG^{+ve} cells of their perivascular niche could represent a clinical approach to treat currently intractable Gr3-MB.

Endothelial cells augment the malignant phenotype of Gr3-MB cells.

To assess possible symbiotic interactions between Gr3-MB stem-like cells and ECs, we used both direct and indirect co-culture systems. While direct culture results in direct physical communication, indirect co-culture solely allows paracrine signaling (Figure.4A). The viability of Gr3-MB cells was improved by both co-culture approaches (Figure.4B). Gr3-MB cells co-cultured in separate compartments from EC cells showed enhanced Hedgehog and TGF-β signaling, and active nucleotide excision repair. Additionally, calcium signaling, which mediates degradation of the extracellular matrix[26] was elevated in co-cultured cells (Figure.4C). ECs co-cultured directly with PRTG^{+ve} cells inhibit actin cytoskeletal organization and cellular tight junction formation, both hallmarks of epithelial to mesenchymal transition (Figure.4D). Direct contact with blood vessels increased stem cell-like phenotypes in Gr3-MB cells, along with upregulation of drug transporters and Glutathione transferase activity (Figure.4E). Both in-direct and direct interaction enhanced endoplasmic-reticulum-associated protein degradation in MB cells, assisting the clearance of misfolded proteins (Figure.4F). To validate these observations, MB cells were cultured as either direct or indirect co-cultures, with or without ECs. Co-culture of Gr3-MB cells with EC cells drives elevated expression of both stem-like and malignancy markers such as: SOX2, CD44 and VIM, as well as Ki67 in the Gr3-MB cells. (Figure.4G). PRTG and other markers showed a marked specific upregulation after direct co-culture with EC cells, mimicking spatial proximity to the physiologic RL^{-}IVP (Figure.4H). Gr3-MB ECs specifically express VWF, ANGPT and COL4A1; ligands that were predicted to signal to Gr3-MB PRTG^{high} stem cells (Figure.S5G). Cumulatively, these results are consistent with a model in which bidirectional intercellular signaling between immature ECs/RL-IVP and PRTG^{high} stem cells maintain a mutually nourishing neurovascular niche that sustains the phenotype of both cell types, in both development and Gr3-MB.

PRTG^{+ve} Gr3-MB stem cells and niche specific endothelial cells establish a co-dependent neurovascular niche.

The Gr3-MB specific EC markers- PLVAP, COL4A, CD34 and SPARC are involved in angiogenesis, cell migration, and adhesion. Increased expression of Gr3-MB EC markers in HUVEC cells after direct co-culture with Gr3-MB cells supports a model in which Gr3-MB cells interact with local ECs to establish and maintain a symbiotic perivascular niche (Figure 5A, B). Additionally, elevated Gr3-MB EC markers COL4A and ENG were detected in ECs surrounding Gr3-MB tumor xenografts, as compared to adjacent non-tumor regions (Figure. 5C–F) indicating that Gr3-MB tumor cells influence the local vasculature.

The human 4V-CP is precisely located, immediately ventral to, and juxtaposed to the RL^{VZ} (Figure. 5G). The CP manufactures the cerebrospinal fluid, as well as secreting proteins that are essential for neuroepithelial proliferation, lineage specification and migration[27]. Our data demonstrates that genes specific to the Gr3-MB endothelium are also highly expressed in 4V-CP. We undertook indirect co-culture of Gr3-MB cells with ECs from the 4V-CP of E16.5 embryos (Figure. 5G and Figure.S5H), demonstrating increased expression of Vimentin, CD44 and SOX2 after co-culture (Figure. 5H, I). Furthermore, Gr3-MB PDX cells co-cultured with E16.5 4V-CP ECs in separate compartments demonstrate increased tumor engraftment compared to control cells (Figure.5J). These results support a model in which both physiological RL^{VZ} and malignant Gr3-MB cells are simultaneously sandwiched and sustained by the flanking 4V-CP and RL- IVP.

Depletion of the PRTG^{+ve} compartment reduces Gr3-MB

To determine if the PRTG^{+ve} compartment of Gr3-MB is necessary to sustain the tumor *in vivo*, as opposed to tumor initiation, we depleted the PRTG^{+ve} compartment of established Gr3-MB *in vivo* using the Diphtheria Toxin receptor (DTR) system. Diphtheria toxin (DT) is known to cross the blood brain barrier, and cells without DTR are insensitive to lower dosages of DT[28]. We xenografted Gr3-MB PDXs transduced with the DTR cDNA downstream of the PRTG promoter into NSG mice (Figure.6A). After tumor establishment, mice were treated with diphtheria toxin (Figure.6B). Administration of DT *in vivo* leads to prolonged survival in two distinct Gr3-MB PDXs (Figure.6C, D) as compared to untreated controls. Residual tumors from treated animals demonstrate diminished PRTG (Figure.6E). This experiment supports a hierarchical Gr3-MB model with apical PRTG^{+ve} cells critical for tumor maintenance.

PRTG contains multiple extracellular Ig-like and fibronectin III-like domains (Figure.6F, I). We developed a monoclonal antibody (mAb) to the region of PRTG spanning the junction of the Ig and Fib domains. Treating Gr3-MB lines with anti-PRTG antibodies reduced viability *in vitro* (Figure.6F). The inhibitory effect was diminished in shPRTG cells confirming the specificity of the antibody (Figure.6G). Anti-PRTG mAb treatment of two Gr3-MB flank xenografts demonstrates significant therapeutic activity (Figure.6H–K). These results indicate that therapies targeting the actual PRTG protein could treat Gr3-MBs.

Anti-PRTG CAR T-cell therapy targets the apical cells of Gr3-MB

We developed optimal human VH binders to the extracellular domains of PRTG through screening a phage-display library (Figure.7A). A panel of normal tissues from P1 from $Prtg^{eGFP}$ transgenic mice demonstrates that post-natal expression of PRTG is limited, suggesting that a post-natal immunotherapy targeting the $PRTG^{high}$ compartment would be safe (Figure.S6). As the Fib-III domains are critical for PRTG function[5], we screened for binders against D3 (D3-9) and D5 (53, 55, 69) regions (Figure.7B). Identified binders exhibit high specificity for PRTG as shown by flow cytometry (Figure.7C) and enzyme-linked immunosorbent assay (Figure.S7A). Dynamic light scattering and size exclusion chromatography demonstrated that binders do not aggregate and remain as monomers respectively (Figure. S7B, C).

D3 and D5 binders were used to generate second-generation CAR T constructs containing a 4-1BB domain. CAR T-cells carrying LD5-55 and LD5-69 induced cytotoxicity when co-cultured with 293T-PRTG compared to control cells treated with Pan T-cells, but not LD3-9 or LD5-53 (Figure.7D). LD3-9, LD5-53, LD5-55 and LD5-69 CAR T cells incubated *in vitro* with two Gr3-MB lines- D425 and D341 at varying effector: target ratios drive high cell death (Figure.7E and S7E). Additionally, PRTG CAR T-cell specific cytotoxicity was confirmed with significant IFN-γ release in the Gr3-MB cell lines, but absent in HEK293T (Figure.7F). Locoregional delivery is ideal to efficiently deliver cellular immunotherapies to Gr3-MB[29]. To validate these findings in the murine trial, we delivered CAR T-cells into the lateral ventricle of mice with established Gr3-PDXs (Figure.7F). Mice treated with LD5-55 CAR T-cells showed diminished tumor burden (Figure.7G) and longer survival (Figure.7H and 7I) than controls treated with Pan T-cells. Lack of PRTG expression in normal pediatric tissues limits unfavorable side-effects (Figure.S7F). There are currently no approved therapies for recurrent Gr3MB, making anti-PRTG CAR T-cell therapy an attractive candidate to test in clinical trials.

Discussion

Medulloblastomas demonstrate a steep cellular hierarchy, with ‘stem-like cells’ at the apex[30]. Oncogenic phenotypes in pediatric cancers are frequently retained embryonic phenotypes, rather than phenotypes acquired during transformation. We present a model in which normal RL^{VZ} $PRTG^{+ve}$ stem-like cells, and their adjacent $CD34^{+ve}$ RL-IVP is transcriptionally mirrored in Gr3-MB. Physiological $PRTG^{+ve}$ cells in the fetal human RL^{VZ} compartment are MYC^{high}, while $PRTG^{-ve}/MYC^{low}$ cells differentiate into progenitor cells in the RL^{SVZ}. The frequent amplifications and translocations of *MYC* found in Gr3-MB, likely help maintain the RL^{VZ} like-state of the apical stem cells. An accumulation of RL^{VZ} like stem cells in the nodulus would first constitute the apex of a PeRL, and then subsequently on progression a Gr3-MB. Our model further implies that Gr3-MB is initiated as early as first trimester of human pregnancy

The RL is divided by the *Homo sapiens* specific RL-IVP which is present briefly during fetal development and has been suggested to sustain the stem-like niche of the RL^{VZ}. Similarly, Gr3-MBs retain an immature perivascular niche surrounding $PRTG^{+ve}$ cancer stem cells. Children with a defective RL^{-}IVP exhibit hypoplasia of the posterior vermis

(Dandy-Walker malformation)[6], suggesting that the vascular niche supports the growth and maintenance of the RL^{VZ}. While Dandy-Walker syndrome may arise due to a deficiency of the RL-IVP, our data suggest the converse in Gr3-MB in which a persistent RL-IVP maintains $PRTG^{+ve}$ RL^{VZ} stem-like cells. In this model, both normal and transformed RL^{VZ} maintain a symbiotic niche with their local immature ECs. Our direct co-culture data emphasizes that ECs are an important component of the Gr3-MB stem cell niche, as both the cell compartments mutually influence each other's transcriptome. Additionally, the directly anatomically adjacent 4V-CP secretes factors that may complement the functions of the RL-IVP[31]. This model of a mutually interdependent, neurovascular niche implies that targeting either the apical $PRTG^{+ve}$ stem cells, or the tumor endothelia of the Gr3-MB using either CAR T-cells, or other immune directed approaches represent attractive targets for Gr3-MB immunotherapies. PRTG and/or markers of immature ECs (i.e., CD34) could serve as future biomarkers to clinically identify high risk Gr3-MB tumors. As there are currently no targeted therapies available for children with Gr3-MB, our anti-PRTG CAR T-cells represent an exciting therapeutic opportunity that needs to be tested in clinical trials.

Now that the biology of PeRLs and their highly specific location within the nodular lobe of the cerebellum is well-understood, asymptomatic children with lesions in the nodulus will be sporadically and incidentally identified in the clinic during MRI imaging for unrelated indications. As prevention is preferable to cure, in the future we predict the development of post-natal screening tools to detect PeRLS across large populations. Therapies that either immunologically or pharmacologically target $PRTG^{high}$ RL^{VZ} like stem cells, or $TBR2^{+ve}$/$Ki67^{+ve}$ RL^{SVZ} like progenitor cells within PeRLs, might be used to secondarily prevent MB in affected children. While it is possible in our current model that removal, destruction, or differentiation of PeRLs could prevent the emergence of metastatic medulloblastoma, the natural history for children with PeRLS is unknown, and affected children should be managed with utmost care.

Limitations of the study

The human specific features of the rhombic lip (conspicuous anatomic split, RL-IVP, interdependent neurovascular niche, massively recurrent mitosis) are found in both normal development and Gr3-MBs. The phenotypes specific to *Homo sapiens*, and not seen in *Mus musculus* are difficult to study using existing *in vivo* model systems. Indeed, the extent to which these human specific modifications are related to the massive production of glutamatergic neurons in the physiologic human cerebellum is currently unknown. Even more speculatively, the idea that these human specific, recently acquired evolutionary changes in the rhombic lip predisposed our species to develop medulloblastoma may prove extremely difficult to test experimentally. Cerebellar organoids may allow testing of our models in four dimensional systems in the future.

STAR methods

RESOURCE AVAILABILITY

Lead contact—Further information and requests for resources and reagents should be directed to and will be fulfilled by the lead contact, Michael Taylor (mdt.cns@gmail.com).

Materials availability—All unique materials and reagents generated in this study can be obtained from the Lead Contact

Data and code availability

- All datasets generated in this study have been deposited and are publicly available as of the date of publication as follows: The data for the single-cell RNA-seq generated from sorted PDX lines, RNA-seq of shNT/shPRTG Gr3-MB cell lines and mouse total tumor RNA-seq referenced in this study are available in the GEO database under the accessions GSE206899. The RNA-seq data for the coculture studies is available under the GEO accession GSE237381. The mass spectrometry proteomics data have been deposited to the ProteomeXchange Consortium via the PRIDE[32] partner repository with the dataset identifier PXD034890.

  Single-nucleus RNA sequencing data from the developing human cerebellum (9PCW-20PCW) was obtained through correspondence from Aldinger et al.[4] and is also available through the Human Cell Atlas (https://www.covid19cellatlas.org/aldinger20) and the UCSC Cell Browser (https://cbl-dev.cells.ucsc.edu). Single-cell RNA seq data used for the Gr3-MB tumor samples was obtained from the European Genome-Phenome Archive (EGA) database under the accession code EGAS00001005826[25]. CS12 human hindbrain scRNA-seq was obtained from the Brain Initiative Cell Census Network (BICCN) and the data is available in NeMO Repository at https://assets.nemoarchive.org/dat-0rsydy7[33].

- This study did not generate any unique code requiring deposition.

- For all additional information, requests for resources and reagents should be directed to and will be fulfilled by the Lead Contact, Dr. Michael Taylor (mdt.cns@gmail.com).

EXPERIMENTAL MODEL AND STUDY PARTICIPANT DETAILS

Human fetal tissue (ISH Study)—Human cerebellar samples used in this study were obtained in accordance with institutional review board guidelines at Seattle Children's Research Institute. Ancestry, race and ethnicity restrictions were neither considered nor used as classification variables in our study. All normal developing human cerebellar tissue utilized in this study was procured by the Millen lab from two distinct tissue repositories: the Human Developmental Biology Resource (HDBR), situated in London and Newcastle, UK, funded by the Medical Research Council (MRC), and the Birth Defects Research Laboratory (BDRL), located at the University of Washington, Seattle, supported by the National Institutes of Health (NIH). All samples were acquired in compliance with approved Institutional Review Board protocols at Seattle Children's Research Institute (SCRI), following project registration at both research centers. Tissues were collected on a regular basis at both centers. Hindbrain tissue collected for histopathology was preserved in formalin (pH 7.6) for approximately one month before being embedded in paraffin. Sagittal sections, measuring 4-5 μm in thickness, were generated using a microtome (Leica RM

2135) and then mounted on Superfrost Plus white slides (VWR International, USA). These slides were stored at room temperature until the immunostaining process was carried out. For RNAseq experiments, fresh hindbrain tissue collected was frozen on dry ice and stored at −80 C. The transfer of tissue was governed by a Material Transfer Agreement (MTA) between the Millen lab (SCRI) and HDBR/BDRL. Appropriate consent was taken prior to sample collection in accordance with strict legal and ethical guidelines.

Medulloblastoma cell lines and patient derived xenografts—All samples used in this study were obtained with informed consent of patients (Ancestry, race and ethnicity restrictions were neither considered nor used as classification variables in our study). All experimental procedures were performed in accordance with the Research Ethics Boards at The Hospital for Sick Children (Toronto, Canada). MB002, D425, D341 (Gr3-MB lines) were kindly provided by Robert Wechsler-Reya lab, Sanford Burnham Prebys, Medical Discovery Institute, La Jolla, California. PDX lines: Med-411FH Med-211FH and Med-114FH (Gr3-MB) generated by the Olson lab, Fred Hutchinson Cancer Research Center, Seattle, WA, USA. MB051 is an in-house line derived from a posterior fossa tumor of a 3.75-year-old Gr3-MB male patient. PDX lines Med 411-FH, Med 211FH and MB051 were passaged by implanting into the cerebella of NSG mice without in vitro passaging. The identity of each line was validated by short tandem repeat (STR) analysis. Pooled HUVEC (Human umbilical vein endothelial cells) were purchased from Promocell.

Mouse Housing and Husbandry—All animal procedures were approved and performed in adherence to guidelines of The Centre for Phenogenomics (Toronto) under the AUPS: AUP25-0100H and 26-0151H. Mice were provided ad libitum access to water and standard chow with 12-hr light/dark cycles and were monitored for health and activity daily. For timed pregnancy, embryos from CD1 female mice the following gestational time points E9.5, E10.5, E11.5, E12.5, and P2 were collected. The morning of the day on which the vaginal plug was detected was designated as E0.5. Features were matched to known developmental hallmarks. NOD-SCID-IL2Rγ null (NSG) and CD1 mice were obtained from TCP in house breeding colony. Prtg-eGFP mouse line (RRID: MMRRC_030365-UCD) was purchased from Mutant Mouse Resource and Research Center (MMRRC) at University of California at Davis, an NIH-funded strain repository, and was donated to the MMRRC by Nathaniel Heintz, Ph.D., The Rockefeller University, GENSAT. Prtg-cre line is a custom made Piggy-Bac transgenic mouse (Cyagen, USA). A plasmid carrying −5kb to +100bp of PRTG promoter followed by -cre was integrated using PiggyBac system. The transgenic plasmid was injected into the pronucleus of fertilized eggs and implanted into surrogate C57BL/6 mothers. This transgenic technique ensures single copy integration with consistent expression of the transgene. The founders were identified by genotyping.

METHOD DETAILS

Cell culture condition—MB cells were grown in Neurocult neurobasal medium (Stem cell tech) containing N2 and B27 supplements (1:100, 1:50; Thermofisher) with basic FGF (10 ng/ml; Peprotech), epidermal growth factor (EGF) (10 ng/ml; Sigma), 2 mM GlutaMAX (Thermofisher), 0.1 mM non-essential amino acids (Wisent labs) 1.0 mM sodium-pyruvate (Wisent labs) and Antibiotic-Antimycotic (Thermofisher) in low adherent plates. Cells were

dissociated with Accutase (Innovative cell tech). For differentiation, the cells were plated in Neurocult medium with 2% FBS for a period of 14 days. HUVEC were cultured in Endothelial Cell Growth Medium (ECGM, Promocell) and between 2-8 passages were used for the experiments. Diluted (50%) Trypsin/EDTA-0.25% in PBS (Wisent labs) was used for dissociation.

Indirect cocultures of HUVEC/CP cells and MB cells were performed in transwell cell culture plates (Corning) with a polycarbonate membrane insert (0.4 μm pore size). Briefly, HUVECs (10,000 cells) were plated in the bottom and MB cells were plated in the insert with ECGM /10% Neurocult at 1:1 ratio. For the control condition, HUVECs or MB cells were plated alone in the same medium. For the direct coculture, the BFP tagged HUVEC cells were mixed with MB cells (mCherry/GFP) at 4:1 ratio and plated on an adherent plate (Corning) in ECGM /10% Neurocult (1:1). The cells were grown for 5 days, viability and flow analysis were performed in technical and biological triplicates. Media was replenished alternate day. For RNA-seq experiments, cells were cocultured for 7 days.

The 4th ventricle choroid plexus (CP) tissue was dissected from E16.5 embryos of FVB/NJ mouse. Tissue was transported in cold Hanks' Buffer+ 0.6% Glucose. Digestion was performed with 1mg/mL Collagenase: 0.1U/mL, Dispase: 0.8U/mL (Sigma-Aldrich) with 50 μg/mL DNAse I (Thermofisher) solution at 37°C for 40 min with intermittent tapping. The preparation was passed through 70-micron filter and flow-sorted using CD31 antibody (R&D systems, Cat AF3628). The cells were washed with dPBS twice by centrifuging at 400g x5min and plated in complete ECGM on adherent plate (Corning). Cells were dissociated with Accutase after 5th day and maintained in ECGM containing 10ng/ml bFGF for 10 days before plating for the experiments.

In situ hybridization—RNAscope assays were performed using commercially available from Advanced Cell Diagnostics. Protocols recommended by the manufacturer were used without modification. Sections were counterstained using Hemotoxylin.

PRTG cell depletion—For Diptheria toxin treatment to deplete DTR-expressing cells, the Gr3-MB lines were transduced with pPRTG-DTR lentivirus. After successful implantation and tumor growth detected by BLI, mice received diphtheria toxin (Sigma-Aldrich, D0564, 40ng i.p) 3 times a week for 3 weeks.

SC tumors: 0.5x10*6 MB cells with 1:1 matrigel (Corning) were injected into the right flank of 6–8-week-old female NSG mice. The mab treatment was started once all the animals showed palpable tumors. Anti-PRTG mab-100ug (Sino biological) in PBS or mIgG (R&D systems) was given intratumorally three times a week for 21 days. The tumor size was measured by BLI.

CAR T in vivo treatment: Single dose of Pan T cells or PRTG CAR-T cells at 1x10*6 cells in 3μl total volume were stereotactically injected into the lateral ventricle of mice using the following co-ordinates: 0.5mm posterior from bregma, 1mm lateral and 3mm deep.

In vivo bioluminescence imaging—Mice were intraperitoneally administered 150 mg/kg D-Luciferin (Perkin Elmer) 5 min before imaging. Animals were anesthetized with 2% isoflurane, and BLI signal was captured using Xenogen Spectrum (IVIS-200). The total flux in radiance of the region of interest was calculated using Living image software.

Confocal immunostaining—Embryos were fixed in 4% paraformaldehyde overnight at 4 °C followed by 15% sucrose (Sigma-Aldrich). Then embryos were snap frozen in O.C.T. medium and placed at −80 °C. Blocks were sectioned at 10 μm thickness and mounted on Microscope Slides (Superfrost Plus). Slides were incubated with 0.1-0.2% Triton X100 (Sigma-Aldrich) and 5% BSA (Bovine Serum Albumin- Sigma-Aldrich) for 1 hr at room temperature. Then slides were incubated with primary antibody diluted in antibody buffer (0.1% Triton X and 3% BSA) at 4 °C overnight. Sections were then washed three times for 15 min with PBS and incubated with secondary antibody for 1hr at room temperature. Secondary antibodies used: Donkey anti rabbit- Alexa 647 (Thermofisher, 1:800), Donkey anti mouse-Alexa594 (Thermofisher, 1:800), Donkey anti mouse- Alexa 488 (Thermofisher, 1:800). After three final washes, mounted with mounting media (Dako). DAPI (Sigma-Aldrich) was used for nuclear staining. Images were acquired using a Leica SP8 light sheet confocal microscope and processed in Image J software.

Immunohistochemistry and imaging—Immunohistochemistry and immunofluorescence for MB tissues: PRTG (Sigma: HPA032138, 1:500) and CD34 (Dako: M7165; 1:50) were performed on 5um FFPE sections. The sections were treated with heat induced retrieval in Dako target solution, pH 9 (Agilent: S236784-2) followed by an overnight primary antibody incubation. For immunohistochemistry, sections were treated with MACH2 Rabbit-HRP Polymer (BioCare: RHRP520H), detected using NovaRed (Vector: SK-4800), and counterstained with hematoxylin (Vector: H3404). For immunofluorescence detection of PRTG and CD34, sections were treated with Alexa-647 goat anti-rabbit (Invitrogen: A21245; 1:500) and Alexa-568 goat anti-mouse (Invitrogen: A11004; 1:500). The sections were counterstained with DAPI and imaged on the Nikon C2 laser scanning confocal microscope.

Human fetal brain IF: Primary antibodies used in the study were GFAP (Agilent, 1:1000) and CD34 (DAKO, 1:100). Fluorescent labelled secondary antibodies from Thermofisher were used at a dilution of 1:1000 (anti-rabbit Alexa Fluor 488, anti-mouse Alexa Fluor 568). Sections were counterstained with DAPI using Vectashield mounting medium (Vector laboratories).

H/E Staining—FFPE sections were de-paraffinized in xylene and rehydrated in a gradient of ethanol prior to processing. Hematoxylin and Eosin (H&E) staining were carried out as previously described[55].

Mouse tissue dissociation—Fresh xenograft tumor tissue was dissociated with enzyme free cell dissociation solution (Millipore # S014C). All embryonic mouse dissections were performed as previously described[56]. In brief, early hindbrain tissue (E9-E11) was dissected parallel to and immediately below the hindbrain neuroepithelium to separate it from facial and forebrain tissue. The excess tissue was removed moving caudally over the

posterior hindbrain to include isthmus and rhombomeres −1 and part of −2. The tissue was dissociated with the Papain Dissociation System (Worthington Biochemical Corporation) as per manufacturer's instructions. Postnatal cerebella were dissected from P1 pups after meninges removal.

Cell sorting and flow cytometry (binders)—One million cells were labeled with 2 μg of conjugated Anti-PRTG antibody (Novus, Clone ID: OTI2B3, cat no-NBP2-02745, 1:100) at 4°C for 45 min in flow buffer (0.5% BSA in dPBS). Cells were sorted by FACS with control and single colour-stained compensation beads (BD Biosciences) on Aria CFI VBYR. For flow analysis, cells were fixed with 4% PFA, and stained with antibody buffer containing 0.1% Triton X100, 1-3% BSA. The cells were analysed in LSRII CFI VBYR and plotted using FlowJo. Sytox blue was used as viability dye. The percentage of positivity was calculated from biological triplicates.

CHO, 293T and 293T-PRTG cells were used for flow cytometry. Total of 10*6 cells were stained with different VH antibodies at a concentration of 1 μM in 200 uL PBS for 30 min on ice. Washed the cells with 1mL PBS three times and incubated with anti-Flag-PE antibody (1:200, BioLegend) for 30 min on ice. Wash the stained cells with 1 mL PBS three times. Antibody binding was detected on a BD LSR II (San Jose, CA). FACS data analysis was performed using FlowJo_V10_CL.

Soft agar colony assay—Low-melting-point agar (Sigma) was melted and mixed with Neurocult media to make a bottom layer (1%) and top layer containing 0.4% agar. The bottom agar layer was allowed to solidify at room temperature for 10 min. Mixture of 10000 cells in media was laid on top of the bottom agar layer per 2 ml/well (6-well plate). Media with growth factors was replenished every 2 days. Triplicate wells were plated for each condition. Colonies were counted after 3 weeks.

In vitro limited dilution assay—LDAs were performed in a 96-well plate format, with 1, 10 and 20 cells/well. Serial dilutions of MB cells were performed with 36 technical replicates per dose. Fresh media was added to the cells every 4 days. Wells were scored for sphere formation on day 14 in triplicates. Statistical analysis was performed with the Extreme Limiting Dilution Analysis (ELDA) web-based online tool[43].

For in vivo tumorigenic assay, indicated numbers of sorted $PRTG^{+ve}$ and $PRTG^{-ve}$ cells were injected into NSG mice and animals were followed for tumor growth by bioluminescence imaging. Humane endpoint was determined based on the physiological condition of the animal. Endpoints were assessed and determined by technicians blinded to experimental groups.

Medulloblastoma and control cell lines were seeded at a density of 2000 cells in 96 well plates (Corning) for dose-response analysis. Twelve hours post seeding, cells were treated with indicated antibodies for 7 days with indicated concentrations. Media was placed every 3rd day with the antibodies. Cell viability was assessed at the end of incubation with Alamar Blue Cell Viability Reagent (Thermofisher).

Tumor model generation—To generate Gr3-MB like tumors, we isolated whole hindbrain cells from E9.5 Prtg-Cre mice or GFP positive cells were flow sorted from E9.5 Prtg–eGFP transgenic hindbrain. These cells were cultured in Neurocult basal medium (Stem cell tech 05700) containing N2 and B27 supplements (1:100, 1:50; Invitrogen) with basic FGF (20 ng/ml; Roche Diagnostics) and EGF (20 ng/ml; Roche). Cells were electroporated with Neon™ Transfection System 10 μL Kit (Thermofisher) as per manufacturer's instruction or infected with the indicated viruses. Cells (100k) were then injected into the cerebella of NSG mice (6–8 weeks old) and followed up by BLI.

Lentiviral production—HEK293T cells were transfected with the 3rd generation helper plasmids pMD2.G, pMDLg pRSV-Rev and transfer plasmid of interest. The supernatant containing the lentiviral particles was collected 48hr after transfection and concentrated 100x using Lenti-X concentrator (Clontech, 631231) as per manufacturers instruction. Viral titer was determined by serial dilution.

Sample preparation for LC MS/MS—All sample preparation, LC MS/MS data collection, and MS data searches were carried out at the SPARC BioCentre at The Hospital for Sick Children (Toronto, ON, Canada). Briefly, the sorted cells were washed in PBS, snap frozen, and stored at −80C until further processing. The pellets were lysed in RIPA buffer (Pierce) with protease and phosphatase inhibitors. Samples were reduced with DTT (10 mM, 60°C, 1 hour), alkylated with iodoacetamide (20 mM, room temperature, 45 min, dark), and digested overnight with trypsin (2 μg; Pierce) at 37°C. Peptides were dried, desalted on C18 ziptips (Millipore) using a DigestPro MSi (Intavis Bioanalytical Instruments) followed by resuspension in Buffer A (0.1% formic acid). Samples were analyzed for an hour by liquid chromatography tandem mass spectrometry (LC-MS/MS) using an EASY-nanoLC 1000 system and Exploris 480 Mass Spectrometer (Thermofisher). The run consisted of an 18 min linear gradient running 3-20% of Buffer A to Buffer B (0.1% Formic acid, 80% acetonitrile), followed by a 31 min linear gradient running 20-35% of Buffer A to Buffer B, a 2 min ramp to 100% Buffer B and 9 min hold at 100% Buffer B, all at a flow rate of 250 nL/min.

MS raw files were analyzed by PEAKS Studio software (Bioinformatics Solutions Inc.) and Proteome Discoverer (version 2.5.0.400)[48], and fragments were searched against Uniprot_UP000005640_Human_15092020.fasta. Search parameters: parent and fragment mass tolerances were set to 10 ppm and 0.02 Da, respectively with a maximum of three missed cleavages, fixed modifications- Carbamidomethylation of cysteine; variable modifications- oxidation of methionine, deamidation of asparagine and glutamine and acetylation of the N-terminus.

Pathway analysis and network generation for mass spectrometry—Pathways were defined by the gene set file Human_GOBP_AllPathways_no_GO_iea_June_20_2019_symbol.gmt that is maintained and updated regularly by the Bader lab (http://download.baderlab.org/EM_Genesets/)[37]. Gene Set size was limited to a range between 10 – 200 and 2000 permutations were carried out. The results of the pathway analysis were visualized using the EnrichmentMap App (v3.3.3)[39] in Cytoscape (v3.8.1)[38]. Network maps were generated for nodes with FDR

q-value < 0.01, p-value < 0.0001 for differential proteomeNodes sharing gene overlaps with Jaccard Coefficient > 0.25 were connected by a green line (edge). Clusters of related pathways were identified and annotated using a Cytoscape app that employs a Markov Cluster Algorithm that connects pathways by shared keywords in the description of each pathway (AutoAnnotate, v1.3.5). The resulting groups of pathways are designated as the major pathways in a circle.

ScFv construction—For protogenin antigen expression, PRTG-Ig (including 4 Ig-like domains), PRTG-Fib (including 5 fibronectin type-III repeats), 5 fibronectin type-III repeats (Domain 1 to domain 5) genes were PCR purified and cloned into pIW-Zeo plasmid with an AviTag and His Tag. For BiTE expression, the anti-PRTG VH antibody genes, anti-CD3 OKT2 scFc gene and Human IgG1 Fc with His Tag were assembled by overlapping PCR and cloned into pIW-Zeo plasmid[34]. Proteins were expressed with Expi293 expression system (Thermofisher) and purified with Ni-NTA columns (Thermofisher). Protein concentration was measured with NanoDrop Lite spectrophotometer (Thermofisher) and protein purity was estimated >95% by SDS-PAGE.

VHs (LD3-9, LD5-53, LD5-55 and LD5-69) were in pComb3x vector. All the plasmids were transformed into HB2151 bacteria. Single colonies were picked up to scale up for expression. After 16 hours induced expression with 1 mM IPTG at 30 °C, 200 rpm. Cells were collected and lysed with Polymyxin B (Sigma) at 37°C for 30 min, 200 rpm. Centrifugation at 15000g for 30 min, supernatant was used for VH purification with Ni-NTA Columns (GE Healthcare). Protein concentration was measured with NanoDrop Lite spectrophotometer (Thermofisher) and protein purity was estimated >95% by SDS-PAGE.

Library construction and panning—The phage displayed human VH libraries were described in our previous work and the panning process were described in detail in our previously published protocol[57,58]. Three rounds of panning were performed. The 1mL antibody libraries were blocked with 5% BSA for one hour and incubated with 5 ug biotinylated antigen for 2 hours at RT, 10 rpm agitation. Phages binding to antigens were separated with Dynabeads™ MyOne™ Streptavidin T1 (Thermofisher) and magnetic separator (Dynal). Wash with 0.1% PBST (PBS containing 0.1% Tween-20) 10 times and PBS twice, bound phage particles were directly infection TG1 cell to produce phage for next round. For the second round of panning 1ug biotinylated antigen was used. After the third round of panning with 0.5 μg biotinylated antigen, individual clones were screened for binding PRTG domains by monoclonal ELISA Screening. Positive clones were selected and sequenced.

P Cell culture and stable cell pool selection: CHO cells were maintained with F12 medium containing 10% FBS. 293T cells and cell lines derived from 293T cells were maintained with DMEM containing 10% FBS. Subcultures were carried out every 2-3 days. Expi293TM cells were maintained with Expi293™ Expression Medium according to the manufacture's protocol.

For PRTG extracellular displayed stable cell line (293T-PRTG) generation. The PRTG extracellular gene with a transmembrane domain was cloned into pIW-Zeo plasmid and

transfected into 293T cells. Transfected cells were selected in DMEM containing 10% FBS and 500 μg/mL Zeocin medium for 7 days to get the stable cell. Stable cells were maintained in medium with 100 μg/mL Zeocin.

ELISA—Ninety-six-well ELISA plates (Corning 3690) were coated with 50 μl antigen at a concentration of 5 ug/ml (diluted with 1x PBS) and incubated at 4°C overnight. On the next day, blocking the plates with 150 μL 5% milk (Bio-RAD) in dPBS solution (5% PBS-Milk) at room temperature for two hours. Meanwhile, 3-fold serial diluted VH antibodies in 5% PBS-Milk with the highest concentration at 1 μM. After blocking, diluted antibodies were added (50μl per well) into each well and incubated at room temperature for 1 hour. Washed the plates 4 times with 0.05% Tween 1x PBS (PBST) solution using a plate washer (BioTek). Next, added 50 μL anti-Flag-HRP (1:1000 dilution in 5% PBS-Milk, Thermofisher) into each well and incubated at room temperature for 1 hour. After 1 hour incubation, the plates were washed 5 times with PBST. Volume of 50 μL TMB substrate (Sigma) was added into each well, allow 1-2 minutes to develop color, then stop with 50 μL H2SO4 (1M, Sigma) and read the plates at 450 nm absorbance. The ELISA results were analyzed using GraphPad Prism 9.0.2.

Dynamic light scattering (DLS)—VH antibodies were buffer changed with PBS and filtered with a 0.22 μM filter. Antibody concentration was adjusted into 5 mg/mL. 500 μL samples were incubated at 37 °C for DLS. Samples were measured at day 0, day 1, day 3 and day 7 on Zetasizer Nano-ZS ZEN 3600 (Malvern Instruments Limited) to determine the size distributions of protein particles.

Size exclusion chromatography (SEC)—A volume of 200 μL (1 mg/mL) filtered samples were used for analysis. Superdex 200 Increase 10/300 GL chromatography (GE Healthcare, Cat. No. 28990944) was used. The column was calibrated with protein molecular mass standards of Ferritin (440 kDa), Aldolase (158 kDa), Conalbumin (75 kDa), Ovalbumin (44 kDa), Carbonic anhydrase (29 kDa), Ribonuclease A (13.7 kDa). Protein was eluted by DPBS buffer at a flow rate of 0.5 mL/min.

CAR T cell generation—For CAR T experiments, the anti-PRTG VH antibody genes were cloned into pLVX-IRES-ZsGreen1 plasmid. The recombinant lentivirus expressing the anti-PRTG CARs were packaged by co-transfecting 293T cells with recombinant plasmids pLVX-CAR-IRES-ZsGreen1, psPAX2 and pMD2.G. The protocol for packaging, concentration and purification of the recombinant lentivirus was addgene lentivirus production protocol.

Human Peripheral Blood Pan-T Cells (Stem cell Tech, # 200-0046) were used for CAR In vitro cytotoxicity Assay. Pan T cells were first activated with anti-CD3/CD28 beads for 48 hours. Activated T cells were mixed with CAR-recombinant lentiviruses at a multiplicity of infection (MOI) value of 20 in the presence of 8 μg/mL polybrene. Cell culture plates were then centrifuged at 800 × g for 1.5 hours at 32°C, incubated for 12 hours in 37°C cell culture incubator, replaced with fresh medium and cultured for 3–4 days for expansion till viability >70%. Transduced cells were examined for GFP expression by Flow cytometry.

In vitro Cytotoxicity Assay for CAR T-cells—CAR T to 293T and 293T-PRTG cells. Anti-PRTG CAR-T cells (effector cells) and blank Pan T cells were incubated with 293T and 293T-PRTG cells at the effector: target ratios of 1.25:1, 2.5:1, 5:1, 10:1 and 20:1 for 48 h in a 96-well cell culture plate (Corning). The co-cultures of CAR-T cells with 293T cells and blank Pan T cells with 293T-PRTG cells were used as negative controls. Cytotoxicity was determined by detecting specific lactate dehydrogenase (LDH) released into the medium from the target cells with the cytotoxicity LDH detection kit (Promega) according to the manufacturer's instructions. Percent cytotoxicity was calculated with the following formula: Cytotoxicity (%) = (Experimental lysis − Effector spontaneous lysis − Target spontaneous lysis)/ (Target maximum lysis − Target spontaneous lysis) × 100%.

CAR T-cells to D341 and D425 cells: Anti-PRTG CAR-T cells (effector cells) and blank Pan T cells were incubated with D425 cells at the effector: target ratio of 10:1. Anti-PRTG CAR-T cells (effector cells) and blank Pan T cells were incubated with D341 cells at the E:T ratio of 4:1. Cultures were maintained till all the T cells reach cell death, stained the cells with trypan blue to determine D341 and D425 cell density under microscope with hematocytometer. The viability was analyzed in biological triplicates.

RNA isolation and quantitative reverse transcription PCR—The total RNA was extracted with RNeasy kit (Qiagen, 74004) as per manufacturer's instructions and quantified by Qubit™ RNA high sensitivity (HS) (Thermofisher, Q32852). qRT-PCR was performed using SYBR Green PCR Master Mix (Applied Biosystems). Ct values obtained from QuantStudio (Applied biosystems) normalized to the housekeeping gene GAPDH and presented as 2-ΔΔCt.

Single cell RNA sequencing (Gr 3-MB sorted cells)

Single cell-RNA library preparation and sequencing: Fresh Medulloblastoma PDX tumor tissues were mechanically dissociated using Enzyme free Cell Dissociation Solution (Millipore, USA) and sorted after Anti-PRTG antibody surface staining. The number and quality of the single-cell suspension were assessed with Trypan blue. Single-cell GEMs (Gel beads-in-emulsion) were generated by loading approximately 10,000–14,000 cells onto the Chromium Controller using Chromium Single Cell 3′ Gel Bead kit (10X Genomics). Indexed single-cell libraries were constructed followed by reverse-transcription and cDNA amplification of barcoded transcripts with Chromium Single Cell 3′ Library kit and Chromium i7 Multiplex kit (10X Genomics). By using Agilent 2100 Bioanalyzer system, the size, concentration, and quality of the 10X library was evaluated. The libraries were sequenced in Illumina Novaseq sequencing platform.

Alignment of raw reads: 10X Cell Ranger pipeline (v3.1.0) was used to obtain gene read counts[44]. Briefly, using the mkfastq function, raw BCL files were demultiplexed into fastq files. Fastqs were aligned to the reference genome hg19 v3.0.0 using the count function to generate raw gene-barcode count matrices.

Quality control and normalization: Prior to sample integration, quality control was performed at an individual sample level. Based on outlier mitochondrial content (due to

cellular damage) or gene counts, low quality cells were determined and excluded from further analysis using the R package Seurat (v4.0.2)[42]. Genes expressed in less than 10 cells were also removed.

Regulon activity analysis—Raw counts from the single cell data were used as input for the Single Cell Regulatory Network Inference and Clustering (SCENIC 1.2.4)[49] R package pipeline. GENIE3[51] was used to infer gene co-expression networks within each cell and combined with the human Rcis Target database included with SCENIC to identify transcription factor targets among the genes. Next, TF networks were binarized as "on/1" or "off/0" with automatic AUCell thresholds. To highlight differences in transcription factor activity, networks that were present in at least 25% of cells in either the PRTG positive or negative samples and had a variance over 0.01 were plotted.

Bulk RNA sequencing on Gr3-MB cell lines and mouse tumors

RNA library preparation and sequencing: RNA samples were quantified by qubit RNA kit (Life Technologies, USA) and quality was assessed by Agilent Bioanlyzer (Agilent technologies, USA). Ribosomal RNA was depleted using Ribo-zero Gold rRNA beads (Illumina, USA), following by purification of RNA fragments. All were converted into cDNA library using TruSeq Stranded Total RNA kit (Illumina, USA) using manufacturer's instructions. Size of the final cDNA libraries were evaluated using Tape station (Agilent, USA) and concentrations were confirmed by qPCR (Kapa Biosystems/Roche). Normalized libraries were pooled, denatured with 0.2N NaOH and diluted to a final concentration of 250 pM. Libraries were loaded onto an Novaseq V1.5 cartridge (Iluumina, USA) and sequenced on Novaseq 6000 instrument (Illumina). Paired end 101 bp protocol to achieve ~ 50 million reads per sample.

RNA sequencing analysis—Quality assessment of the raw reads was carried out using the FastQC tool (version 0.11.5)[41]. The reads were aligned to the human reference genome GRCh38 using Star aligner (version 2.4.2a)[35]. The RNA-Seq reads were counted over gene exons using HtSeq (version 0.11.0)[45]. Genes were annotated as per the Gencode Version 33 annotation file (https://www.gencodegenes.org/human/release_33.html). DEseq2 (DESeq2_1.26.0)[36] was used for normalization and differential gene expression analysis.

The reads from mouse tumors were aligned to GRCm38 (mouse reference genome) using star aligner (version 2.4.2a). The RNA-Seq reads of exons were counted using HtSeq (version 0.11.0). Genes were annotated as per the annotation file of Gencode (Version M25) (https://www.gencodegenes.org/mouse/release_M25.html).

Inter-species tumor clustering—Human genes and corresponding Mus musculus orthologs were downloaded from ensemble biomart (http://www.ensembl.org/biomart/martview). Raw Htseq read counts of orthologous genes in human medulloblastoma tumors from ICGC cohort[12] and mouse were combined. variance stabilizing transformation method by DEseq2 (DESeq2_1.26.0)[36] was used for normalization. Unsupervised clustering was performed on merged RNA-seq cohorts after ComBat batch effect adjustment[50] with top 500 variable genes.

Hybridoma maintenance and antibody purification—Murine hybridoma cell line, which produces a monoclonal antibody specific for the human PRTG was obtained from Sinobiological. Inc, China. Cells were maintained in 15% FBS in Hybridoma SF media (Thermofisher, 12045076). Antibody were purified from mass culture supernatants by NAb™ Protein A/G Spin Column (Thermofisher, 89958) according to the manufacturers' protocols. Antibody concentration was determined by OD280, and purity was assessed by SDS-PAGE.

Single-cell RNA sequencing (CS12 human fetal brain)

Sample collection and processing: Single-cell RNA-sequencing data for the human fetal hindbrain at Carnegie Stage 12 was obtained from the Brain Initiative Cell Census Network (BICCN)[33]. Library preparation was performed with the 10X Chromium v2 chemistry as described previously. Reads were trimmed, demultiplexed, aligned to the GRCh38-0.1.2 reference genome, and unique transcripts were counted using CellRanger v2. The output gene by cell counts were downloaded from the Neuroscience Multi-Omic (NeMO) Archive, accessible at the following URL: http://data.nemoarchive.org/biccn/grant/u01_devhu/kriegstein/transcriptome/scell/10x_v2/human/processed/counts/. Downstream data processing was performed in R 3.6.1[40] using methods from the Seurat package (v.3.2.1)[42]. Genes with expression in fewer than 3 cells and cells with fewer than 200 detected genes were excluded. Low quality cells were filtered based on the following metrics: number of detected genes, number of unique molecular identifiers (UMIs), and percent of mitochondrial transcripts. Libraries were scaled to 10,000 UMIs per cell and log-normalized. Number of UMIs and mitochondrial content were regressed from the normalized gene counts and the residuals were z-scored gene-wise. Dimensionality reduction was performed using principal component analysis (PCA), with 100 PCs computed using the top 2,000 most variant genes. The first 30 PCs were then used as input for visualization in two dimensions using uniform manifold approximation and projection (UMAP)[52] and t-distributed stochastic neighbor embedding (t-SNE)[53]. Cells were clustered by constructing a Shared Nearest Neighbor (SNN) graph from the first 30 PCs and applying the Louvain algorithm for community detection, with the resolution parameter set to 1.0. Cell cycle scores for G2/M and S phases were computed as implemented in Seurat, by calculating the average expression of G2/M and S phase-associated gene lists in each single cell and subtracting the average expression of control gene lists[59]. Control gene lists were derived by binning genes in each input list into 24 bins according to expression levels and randomly selecting 100 control genes from within each expression bin. To classify cells according to their degree of differentiation, we applied CytoTRACE algorithm which estimates the differentiation state of single cells using the number of genes expressed per cell[46].

Mapping transcriptional similarity between medulloblastoma and the human cerebellum—We used the CHETAH package (v1.1.4)[47] to map transcriptional similarities between MB and human cerebellum at CS12. Briefly, CHETAH uses a self-defined metric called "confidence score" calculated by the Spearman correlation. We used ngenes=200 and confidence score=0.01. Cells that were not confidently assigned to a final cell type

(nodes) were considered as unassigned. Cell type predictions were projected into UMAP embeddings.

Cell-cell communication analysis—To identify putative ligand–receptor interactions between Gr3-MB stem cells and endothelial cells in our scRNA-seq data, we used CCInx (v0.4)[54]. We used the BuildGeneStatList function to calculate scaled expression levels of ligands in endothelial cells and receptors in Gr3-MB stem cells. The list of interactions was determined using the built-in curated database of ligand–receptor interactions (https://baderlab.org/CellCellInteractions). Edges represent putative interactions, and they are ordered and colored by the magnitude of the average expression of the ligand and receptor.

Single-nucleus RNA sequencing (PCW9-20 human fetal samples)—Human cerebellar tissue from PCW9-20 and were previously obtained and processed for single-nucleus RNA sequencing[4]. Samples were aligned to human reference genome hg19.

Quantification and Statistical Analysis—The statistical test and significance were reported in the figure legends. A two-sided log-rank T-test was used for the Kaplan-Meier survival analysis. Two-tailed Student T-test or one-way ANOVA was used to calculate viability, cytotoxicity, flow cytometry statistics.

Supplementary Material

Refer to Web version on PubMed Central for supplementary material.

Authors

Abhirami Visvanathan[1,2,†], Olivier Saulnier[1,2,3,4,5,†], Chuan Chen[6,7,8,†], Parthiv Haldipur[9], Wilda Orisme[10], Alberto Delaidelli[11], Seungmin Shin[6,7,8], Jake Millman[9], Andrew Bryant[12], Namal Abeysundara[1,2], Xujia Wu[13], Liam D Hendrikse[1,2,14], Vikas Patil[15], Zahedeh Bashardanesh[16], Joseph Golser[9], Bryn G. Livingston[1,2,17], Takuma Nakashima[18], Yusuke Funakoshi[18], Winnie Ong[1,2,17], Alexandra Rasnitsyn[1,2,14], Kimberly A. Aldinger[19], Cory M Richman[1,2,14], Randy Van Ommeren[1,2,17], John J.Y. Lee[1,2,17], Michelle Ly[1,2,17], Maria C. Vladoiu[1,2,17], Kaitlin Kharas[1,2,17], Polina Balin[1,2,17], Anders W. Erickson[1,2,17], Vernon Fong[1,2,17], Jiao Zhang[1,2,20,21], Raúl A. Suárez[1,2], Hao Wang[1,2], Ning Huang[1,2], Jonelle G Pallota[1,2], Tajana Douglas[1,2], Joonas Haapasalo[22], Ferechte Razavi[23], Evelina Silvestri[24], Olga Sirbu[1,2,14], Samantha Worme[25], Michelle M. Kameda-Smith[20,21], Xiaochong Wu[1,2,20,21], Craig Daniels[1,2,20,21], Antony K MichaelRaj[26], Aparna Badhuri[27], Daniel Schramek[28], Hiromichi Suzuki[18], Livia Garzia[29], Nabil Ahmed[30], Claudia L Kleinman[31,32], Lincoln D Stein[33,34], Peter Dirks[1,2,34,35], Christopher Dunham[36], Nada Jabado[37,38], Jeremy N Rich[13], Wei Li[6,7,8], Poul H Sorensen[11], Robert J. Wechsler-Reya[39], William A. Weiss[40,41,42], Kathleen J. Millen[43], David W. Ellison[10], Dimiter S Dimitrov[6,7,8,*], Michael D. Taylor[1,2,14,17,20,21,44,45,46,47,*]

Affiliations

[1.]The Arthur and Sonia Labatt Brain Tumour Research Centre, The Hospital for Sick Children, Toronto, Ontario, Canada

[2.]Developmental & Stem Cell Biology Program, The Hospital for Sick Children, Toronto, Ontario, Canada

[3.]Genomics and Development of Childhood Cancers, Institut Curie, PSL University, 75005 Paris, France

[4.]INSERM U830, Cancer Heterogeneity Instability and Plasticity, Institut Curie, PSL University, 75005 Paris, France

[5.]SIREDO: Care, Innovation and Research for Children, Adolescents and Young Adults with Cancer, Institut Curie, 75005 Paris, France

[6.]Center for Antibody Therapeutics, University of Pittsburgh School of Medicine, Pittsburgh, United States

[7.]Division of Infectious Diseases, University of Pittsburgh School of Medicine, Pittsburgh, United States

[8.]Department of Medicine, University of Pittsburgh School of Medicine, Pittsburgh, United States

[9.]Center for Integrative Brain Research, Seattle Children's Research Institute, Seattle, Washington, United States

[10.]St. Jude Children's Research Hospital, Memphis, Tennessee, United States

[11.]British Columbia Cancer Agency, Vancouver, BC, Canada

[12.]Department of Pathology, St. Jude Children's Research Hospital, Memphis, Tennessee, United States

[13.]Hillman Cancer Center, University of Pittsburgh Medical Center, Pittsburgh, Pennsylvania, United States

[14.]Department of Medical Biophysics, University of Toronto, Toronto, Ontario, Canada

[15.]MacFeeters-Hamilton Center for Neuro-Oncology Research, Princess Margaret Cancer Centre, University Health Network, Toronto, Ontario, Canada

[16.]Lady Davis Institute, McGill University, Montreal, Quebec, Canada

[17.]Department of Laboratory Medicine and Pathobiology, University of Toronto, Toronto, Ontario, Canada

[18.]Division of Brain Tumor Translational Research, National Cancer Center Research Institute, Tokyo, Japan

[19.]Departments of Pediatrics and Neurology. University of Washington, Seattle, United States

[20]Texas Children's Cancer and Hematology Center, Houston, TX, United States

[21]Department of Pediatrics – Hematology/Oncology, Baylor College of Medicine, Houston, TX, United States

[22]Department of Neurosurgery, Tampere University Hospital, Tampere, Finland

[23]Assistance Publique Hôpitaux de Paris, Hôpital Necker-Enfants Malades, Paris, France

[24]Surgical Pathology Unit, San Camillo Forlanini Hospital, Rome, Italy

[25]Division of Experimental Medicine, McGill University, Montreal, Quebec, Canada

[26]Department of Neurological Surgery, University of Pittsburgh School of Medicine, Pittsburgh, United States

[27]Department of Biological Chemistry, David Geffen School of Medicine at UCLA, Los Angeles, California, United States

[28]Centre for Molecular and Systems Biology, Lunenfeld-Tanenbaum Research Institute, Sinai Health System, Toronto, Ontario, Canada

[29]Cancer Research Program, McGill University Health Centre Research Institute, Montreal, Quebec, Canada

[30]Centre for Cell and Gene Therapy, Texas Children's Hospital, Houston Methodist Hospital, Baylor College of Medicine, Houston, TX, United States

[31]Department of Human Genetics, McGill University, Montreal, Quebec, Canada

[32]Lady Davis Research Institute, Jewish General Hospital, Montreal, Quebec, Canada

[33]Adaptive Oncology, Ontario Institute for Cancer Research, Toronto, Ontario, Canada

[34]Department of Molecular Genetics, University of Toronto, Toronto, Ontario, Canada

[35]Division of Neurosurgery, The Hospital for Sick Children, Toronto, Ontario, Canada

[36]British Columbia Children's Hospital, Vancouver, Canada

[37]Departments of Pediatrics and Human Genetics, McGill University, Montreal, Quebec, Canada

[38]The Research Institute of the McGill University Health Center, Montreal, Quebec, Canada

[39]Tumor Initiation and Maintenance Program, NCI-Designated Cancer Center, Sanford Burnham Prebys Medical Discovery Institute, La Jolla, California, United States

[40]Department of Neurology, University of California San Francisco, San Francisco, California, United States

[41]Department of Neurological Surgery, University of California San Francisco, San Francisco, California, United States

[42]Department of Pediatrics, University of California San Francisco, San Francisco, California, United States

[43]Department of Pediatrics, University of Washington, Seattle, United States

[44]Department of Neurosurgery, Baylor College of Medicine, Houston, TX, United States

[45]Department of Neurosurgery, Texas Children's Hospital, Houston, TX, United States

[46]Dan L Duncan Comprehensive Cancer Center, Baylor College of Medicine, Houston, TX, United States

[47]Department of Surgery, University of Toronto, Toronto, ON, Canada

Acknowledgements

M.D.T. is a CPRIT Scholar in Cancer Research. M.D.T. is supported by the NIH (R01NS106155, R01CA159859 and R01CA255369), The Pediatric Brain Tumour Foundation, The Terry Fox Research Institute, The Canadian Institutes of Health Research, The Cure Search Foundation, Matthew Larson Foundation (IronMatt), b.r.a.i.n.child, Meagan's Walk, SWIFTY Foundation, The Brain Tumour Charity, Genome Canada, Genome BC, Genome Quebec, the Ontario Research Fund, Worldwide Cancer Research, V-Foundation for Cancer Research, and the Ontario Institute for Cancer Research through funding provided by the Government of Ontario. M.D.T. is also supported by a Canadian Cancer Society Research Institute Impact grant, a Cancer Research UK Brain Tumour Award, and by a Stand Up To Cancer (SU2C) St. Baldrick's Pediatric Dream Team Translational Research Grant (SU2C-AACR-DT1113) and SU2C Canada Cancer Stem Cell Dream Team Research Funding (SU2C-AACR-DT-19-15) provided by the Government of Canada through Genome Canada and the Canadian Institutes of Health Research, with supplementary support from the Ontario Institute for Cancer Research through funding provided by the Government of Ontario. Stand Up to Cancer is a program of the Entertainment Industry Foundation administered by the American Association for Cancer Research. M.D.T. is also supported by the Garron Family Chair in Childhood Cancer Research at the Hospital for Sick Children and the University of Toronto. The authors thank Ben Pakuts for graphic design support.

REFERNCES

1. Northcott PA, Shih DJH, Peacock J, Garzia L, Sorana Morrissy A, Zichner T, Stütz AM, Korshunov A, Reimand J, Schumacher SE, et al. (2012). Subgroup-specific structural variation across 1,000 medulloblastoma genomes. Nature 488, 49–56. 10.1038/nature11327. [PubMed: 22832581]
2. Cavalli FMG, Remke M, Rampasek L, Peacock J, Shih DJH, Luu B, Garzia L, Torchia J, Nor C, Morrissy AS, et al. (2017). Intertumoral Heterogeneity within Medulloblastoma Subgroups. Cancer Cell 31, 737–754.e6. 10.1016/j.ccell.2017.05.005. [PubMed: 28609654]
3. Haldipur P, Aldinger KA, Bernardo S, Deng M, Timms AE, Overman LM, Winter C, Lisgo SN, Razavi, Silvestri E, et al. (2019). Spatiotemporal expansion of primary progenitor zones in the developing human cerebellum. Science (1979) 366, 454–460. 10.1126/science.aax7526.
4. Aldinger KA, Thomson Z, Phelps IG, Haldipur P, Deng M, Timms AE, Hirano M, Santpere G, Roco C, Rosenberg AB, et al. (2021). Spatial and cell type transcriptional landscape of human cerebellar development. Nat Neurosci 24, 1163–1175. 10.1038/s41593-021-00872-y. [PubMed: 34140698]
5. Wong YH, Lu AC, Wang YC, Cheng HC, Chang C, Chen PH, Yu JY, and Fann MJ (2010). Protogenin defines a transition stage during embryonic neurogenesis and

prevents precocious neuronal differentiation. Journal of Neuroscience 30, 4428–4439. 10.1523/JNEUROSCI.0473-10.2010. [PubMed: 20335479]

6. Haldipur P, Bernardo S, Aldinger KA, Sivakumar T, Millman J, Sjoboen AH, Dang D, Dubocanin D, Deng M, Timms AE, et al. (2021). Evidence of disrupted rhombic lip development in the pathogenesis of Dandy–Walker malformation. Acta Neuropathol 142, 761–776. 10.1007/s00401-021-02355-7. [PubMed: 34347142]
7. Cheng Y, Liao S, Xu G, Hu J, Guo D, Du F, Contreras A, Cai KQ, Peri S, Wang Y, et al. (2020). NeuroD1 Dictates Tumor Cell Differentiation in Medulloblastoma. Cell Rep 31, 107782. 10.1016/j.celrep.2020.107782. [PubMed: 32579914]
8. Fan X, Masamsetti VP, Sun JQ, Engholm-Keller K, Osteil P, Studdert J, Graham ME, Fossat N, and Tam PP (2021). TWIST1 and chromatin regulatory proteins interact to guide neural crest cell differentiation. Elife 10. 10.7554/eLife.62873.
9. Wizeman JW, Guo Q, Wilion EM, and Li JY (2019). Specification of diverse cell types during early neurogenesis of the mouse cerebellum. Elife 8. 10.7554/eLife.42388.
10. Chizhikov VV, Lindgren AG, Mishima Y, Roberts RW, Aldinger KA, Miesegaes GR, Currle DS, Monuki ES, and Millen KJ (2010). Lmx1a regulates fates and location of cells originating from the cerebellar rhombic lip and telencephalic cortical hem. Proceedings of the National Academy of Sciences 107, 10725–10730. 10.1073/pnas.0910786107.
11. Yeung J, Ha TJ, Swanson DJ, and Goldowitz D (2016). A Novel and Multivalent Role of Pax6 in Cerebellar Development. Journal of Neuroscience 36, 9057–9069. 10.1523/JNEUROSCI.4385-15.2016. [PubMed: 27581449]
12. Northcott PA, Buchhalter I, Morrissy AS, Hovestadt V, Weischenfeldt J, Ehrenberger T, Gröbner S, Segura-Wang M, Zichner T, Rudneva VA, et al. (2017). The whole-genome landscape of medulloblastoma subtypes. Nature 547, 311–317. 10.1038/nature22973. [PubMed: 28726821]
13. Northcott PA, Lee C, Zichner T, Stütz AM, Erkek S, Kawauchi D, Shih DJH, Hovestadt V, Zapatka M, Sturm D, et al. (2014). Enhancer hijacking activates GFI1 family oncogenes in medulloblastoma. Nature 511, 428–434. 10.1038/nature13379. [PubMed: 25043047]
14. Remke M, Ramaswamy V, Peacock J, Shih DJH, Koelsche C, Northcott PA, Hill N, Cavalli FMG, Kool M, Wang X, et al. (2013). TERT promoter mutations are highly recurrent in SHH subgroup medulloblastoma. Acta Neuropathol 126, 917–929. 10.1007/s00401-013-1198-2. [PubMed: 24174164]
15. Serrano M, Lee H-W, Chin L, Cordon-Cardo C, Beach D, and DePinho RA (1996). Role of the INK4a Locus in Tumor Suppression and Cell Mortality. Cell 85, 27–37. 10.1016/S0092-8674(00)81079-X. [PubMed: 8620534]
16. Northcott PA, Korshunov A, Witt H, Hielscher T, Eberhart CG, Mack S, Bouffet E, Clifford SC, Hawkins CE, French P, et al. (2011). Medulloblastoma Comprises Four Distinct Molecular Variants. Journal of Clinical Oncology 29, 1408–1414. 10.1200/JCO.2009.27.4324. [PubMed: 20823417]
17. Parant O, Dubernard G, Challier J-C, Oster M, Uzan S, Aractingi S, and Khosrotehrani K (2009). CD34+ cells in maternal placental blood are mainly fetal in origin and express endothelial markers. Laboratory Investigation 89, 915–923. 10.1038/labinvest.2009.55. [PubMed: 19488036]
18. Bautch VL (2017). Endoglin moves and shapes endothelial cells. Nat Cell Biol 19, 593–595. 10.1038/ncb3543. [PubMed: 28561054]
19. Wälchli T, Bisschop J, Carmeliet P, Zadeh G, Monnier PP, De Bock K, and Radovanovic I (2023). Shaping the brain vasculature in development and disease in the single-cell era. Nat Rev Neurosci 24, 271–298. 10.1038/s41583-023-00684-y. [PubMed: 36941369]
20. Spatazza J, Lee HHC, Di Nardo AA, Tibaldi L, Joliot A, Hensch TK, and Prochiantz A (2013). Choroid-Plexus-Derived Otx2 Homeoprotein Constrains Adult Cortical Plasticity. Cell Rep 3, 1815–1823. 10.1016/j.celrep.2013.05.014. [PubMed: 23770240]
21. Kompaníková P, and Bryja V (2022). Regulation of choroid plexus development and its functions. Cellular and Molecular Life Sciences 79, 304. 10.1007/s00018-022-04314-1. [PubMed: 35589983]

22. Hunter NL, and Dymecki SM (2007). Molecularly and temporally separable lineages form the hindbrain roof plate and contribute differentially to the choroid plexus. Development 134, 3449–3460. 10.1242/dev.003095. [PubMed: 17728348]

23. Kapur RP, Mahony BS, Finch L, and Siebert JR (2009). Normal and abnormal anatomy of the cerebellar vermis in midgestational human fetuses. Birth Defects Res A Clin Mol Teratol 85, 700–709. 10.1002/bdra.20589. [PubMed: 19441098]

24. Smith KS, Bihannic L, Gudenas BL, Haldipur P, Tao R, Gao Q, Li Y, Aldinger KA, Iskusnykh IY, Chizhikov VV, et al. (2022). Unified rhombic lip origins of group 3 and group 4 medulloblastoma. Nature 609, 1012–1020. 10.1038/s41586-022-05208-9. [PubMed: 36131015]

25. Hendrikse LD, Haldipur P, Saulnier O, Millman J, Sjoboen AH, Erickson AW, Ong W, Gordon V, Coudière-Morrison L, Mercier AL, et al. (2022). Failure of human rhombic lip differentiation underlies medulloblastoma formation. Nature 609, 1021–1028. 10.1038/s41586-022-05215-w. [PubMed: 36131014]

26. Monteith GR, Prevarskaya N, and Roberts-Thomson SJ (2017). The calcium–cancer signalling nexus. Nat Rev Cancer 17, 373–380. 10.1038/nrc.2017.18.

27. Lun MP, Monuki ES, and Lehtinen MK (2015). Development and functions of the choroid plexus–cerebrospinal fluid system. Nat Rev Neurosci 16, 445–457. 10.1038/nrn3921. [PubMed: 26174708]

28. Buch T, Heppner FL, Tertilt C, Heinen TJAJ, Kremer M, Wunderlich FT, Jung S, and Waisman A (2005). A Cre-inducible diphtheria toxin receptor mediates cell lineage ablation after toxin administration. Nat Methods 2, 419–426. 10.1038/nmeth762. [PubMed: 15908920]

29. Spector R, Robert Snodgrass S, and Johanson CE (2015). A balanced view of the cerebrospinal fluid composition and functions: Focus on adult humans. Exp Neurol 273, 57–68. 10.1016/j.expneurol.2015.07.027. [PubMed: 26247808]

30. Vanner RJ, Remke M, Gallo M, Selvadurai HJ, Coutinho F, Lee L, Kushida M, Head R, Morrissy S, Zhu X, et al. (2014). Quiescent Sox2+ Cells Drive Hierarchical Growth and Relapse in Sonic Hedgehog Subgroup Medulloblastoma. Cancer Cell 26, 33–47. 10.1016/j.ccr.2014.05.005. [PubMed: 24954133]

31. Lehtinen MK, Zappaterra MW, Chen X, Yang YJ, Hill AD, Lun M, Maynard T, Gonzalez D, Kim S, Ye P, et al. (2011). The Cerebrospinal Fluid Provides a Proliferative Niche for Neural Progenitor Cells. Neuron 69, 893–905. 10.1016/j.neuron.2011.01.023. [PubMed: 21382550]

32. Perez-Riverol Y, Bai J, Bandla C, García-Seisdedos D, Hewapathirana S, Kamatchinathan S, Kundu DJ, Prakash A, Frericks-Zipper A, Eisenacher M, et al. (2022). The PRIDE database resources in 2022: a hub for mass spectrometry-based proteomics evidences. Nucleic Acids Res 50, D543–D552. 10.1093/nar/gkab1038. [PubMed: 34723319]

33. Eze UC, Bhaduri A, Haeussler M, Nowakowski TJ, and Kriegstein AR (2021). Single-cell atlas of early human brain development highlights heterogeneity of human neuroepithelial cells and early radial glia. Nat Neurosci 24, 584–594. 10.1038/s41593-020-00794-1. [PubMed: 33723434]

34. Chen C, Sun Z, Liu X, Li W, and Dimitrov DS (2021). Protocol for constructing large size human antibody heavy chain variable domain (VH) library and selection of SARS-CoV-2 neutralizing antibody domains. STAR Protoc 2, 100617. 10.1016/j.xpro.2021.100617. [PubMed: 34095859]

35. Dobin A, Davis CA, Schlesinger F, Drenkow J, Zaleski C, Jha S, Batut P, Chaisson M, and Gingeras TR (2013). STAR: ultrafast universal RNA-seq aligner. Bioinformatics 29, 15–21. 10.1093/bioinformatics/bts635. [PubMed: 23104886]

36. Love MI, Huber W, and Anders S (2014). Moderated estimation of fold change and dispersion for RNA-seq data with DESeq2. Genome Biol 15, 550. 10.1186/s13059-014-0550-8. [PubMed: 25516281]

37. Subramanian A, Tamayo P, Mootha VK, Mukherjee S, Ebert BL, Gillette MA, Paulovich A, Pomeroy SL, Golub TR, Lander ES, et al. (2005). Gene set enrichment analysis: A knowledge-based approach for interpreting genome-wide expression profiles. Proceedings of the National Academy of Sciences 102, 15545–15550. 10.1073/pnas.0506580102.

38. Shannon P, Markiel A, Ozier O, Baliga NS, Wang JT, Ramage D, Amin N, Schwikowski B, and Ideker T (2003). Cytoscape: A Software Environment for Integrated Models of Biomolecular Interaction Networks. Genome Res 13, 2498–2504. 10.1101/gr.1239303. [PubMed: 14597658]

39. Merico D, Isserlin R, Stueker O, Emili A, and Bader GD (2010). Enrichment Map: A Network-Based Method for Gene-Set Enrichment Visualization and Interpretation. PLoS One 5, e13984. 10.1371/journal.pone.0013984. [PubMed: 21085593]
40. R version 3.6.0 (The R Project for Statistical Computing) (2014).
41. Andrews S. (2010). FastQC: a quality control tool for high throughput sequence data. Babraham Bioinformatics.
42. Stuart T, Butler A, Hoffman P, Hafemeister C, Papalexi E, Mauck WM, Hao Y, Stoeckius M, Smibert P, and Satija R (2019). Comprehensive Integration of Single-Cell Data. Cell 177, 1888–1902.e21. 10.1016/j.cell.2019.05.031. [PubMed: 31178118]
43. Hu Y, and Smyth GK (2009). ELDA: Extreme limiting dilution analysis for comparing depleted and enriched populations in stem cell and other assays. J Immunol Methods 347, 70–78. 10.1016/j.jim.2009.06.008. [PubMed: 19567251]
44. Zheng GXY, Terry JM, Belgrader P, Ryvkin P, Bent ZW, Wilson R, Ziraldo SB, Wheeler TD, McDermott GP, Zhu J, et al. (2017). Massively parallel digital transcriptional profiling of single cells. Nat Commun 8, 14049. 10.1038/ncomms14049. [PubMed: 28091601]
45. Anders S, Pyl PT, and Huber W (2015). HTSeq--a Python framework to work with high-throughput sequencing data. Bioinformatics 31, 166–169. 10.1093/bioinformatics/btu638. [PubMed: 25260700]
46. Gulati GS, Sikandar SS, Wesche DJ, Manjunath A, Bharadwaj A, Berger MJ, Ilagan F, Kuo AH, Hsieh RW, Cai S, et al. (2020). Single-cell transcriptional diversity is a hallmark of developmental potential. Science (1979) 367, 405–411. 10.1126/science.aax0249. [PubMed: 31974247]
47. de Kanter JK, Lijnzaad P, Candelli T, Margaritis T, and Holstege FCP (2019). CHETAH: a selective, hierarchical cell type identification method for single-cell RNA sequencing. Nucleic Acids Res 47, e95–e95. 10.1093/nar/gkz543. [PubMed: 31226206]
48. Choi M, Chang C-Y, Clough T, Broudy D, Killeen T, MacLean B, and Vitek O (2014). MSstats: an R package for statistical analysis of quantitative mass spectrometry-based proteomic experiments. Bioinformatics 30, 2524–2526. 10.1093/bioinformatics/btu305. [PubMed: 24794931]
49. Aibar S, González-Blas CB, Moerman T, Huynh-Thu VA, Imrichova H, Hulselmans G, Rambow F, Marine J-C, Geurts P, Aerts J, et al. (2017). SCENIC: single-cell regulatory network inference and clustering. Nat Methods 14, 1083–1086. 10.1038/nmeth.4463. [PubMed: 28991892]
50. Leek JT, Johnson WE, Parker HS, Jaffe AE, and Storey JD (2012). The sva package for removing batch effects and other unwanted variation in high-throughput experiments. Bioinformatics 28, 882–883. 10.1093/bioinformatics/bts034. [PubMed: 22257669]
51. Huynh-Thu VA, Irrthum A, Wehenkel L, and Geurts P (2010). Inferring Regulatory Networks from Expression Data Using Tree-Based Methods. PLoS One 5, e12776. 10.1371/journal.pone.0012776. [PubMed: 20927193]
52. Becht E, McInnes L, Healy J, Dutertre C-A, Kwok IWH, Ng LG, Ginhoux F, and Newell EW (2019). Dimensionality reduction for visualizing single-cell data using UMAP. Nat Biotechnol 37, 38–44. 10.1038/nbt.4314.
53. Laurens van der Maaten, and Geoffrey Hinton (2008). Visualizing Data using t-SNE. Journal of Machine Learning Research 9, 2579–2605.
54. Ximerakis M, Lipnick SL, Innes BT, Simmons SK, Adiconis X, Dionne D, Mayweather BA, Nguyen L, Niziolek Z, Ozek C, et al. (2019). Single-cell transcriptomic profiling of the aging mouse brain. Nat Neurosci 22, 1696–1708. 10.1038/s41593-019-0491-3. [PubMed: 31551601]
55. Fischer AH, Jacobson KA, Rose J, and Zeller R (2008). Hematoxylin and Eosin Staining of Tissue and Cell Sections. Cold Spring Harb Protoc 2008, pdb.prot4986. 10.1101/pdb.prot4986.
56. Vladoiu MC, El-Hamamy I, Donovan LK, Farooq H, Holgado BL, Sundaravadanam Y, Ramaswamy V, Hendrikse LD, Kumar S, Mack SC, et al. (2019). Childhood cerebellar tumours mirror conserved fetal transcriptional programs. Nature 572, 67–73. 10.1038/s41586-019-1158-7. [PubMed: 31043743]
57. Sun Z, Li W, Mellors JW, Orentas R, and Dimitrov DS (2022). Construction of a Large Size Human Immunoglobulin Heavy Chain Variable (VH) Domain Library, Isolation and Characterization of Novel Human Antibody VH Domains Targeting PD-L1 and CD22. Front Immunol 13. 10.3389/fimmu.2022.869825.

58. Choudhry V, Zhang M-Y, Sidorov IA, Louis JM, Harris I, Dimitrov AS, Bouma P, Cham F, Choudhary A, Rybak SM, et al. (2007). Cross-reactive HIV-1 neutralizing monoclonal antibodies selected by screening of an immune human phage library against an envelope glycoprotein (gp140) isolated from a patient (R2) with broadly HIV-1 neutralizing antibodies. Virology 363, 79–90. 10.1016/j.virol.2007.01.015. [PubMed: 17306322]

59. Tirosh I, Izar B, Prakadan SM, Wadsworth MH, Treacy D, Trombetta JJ, Rotem A, Rodman C, Lian C, Murphy G, et al. (2016). Dissecting the multicellular ecosystem of metastatic melanoma by single-cell RNA-seq. Science (1979) 352, 189–196. 10.1126/science.aad0501.

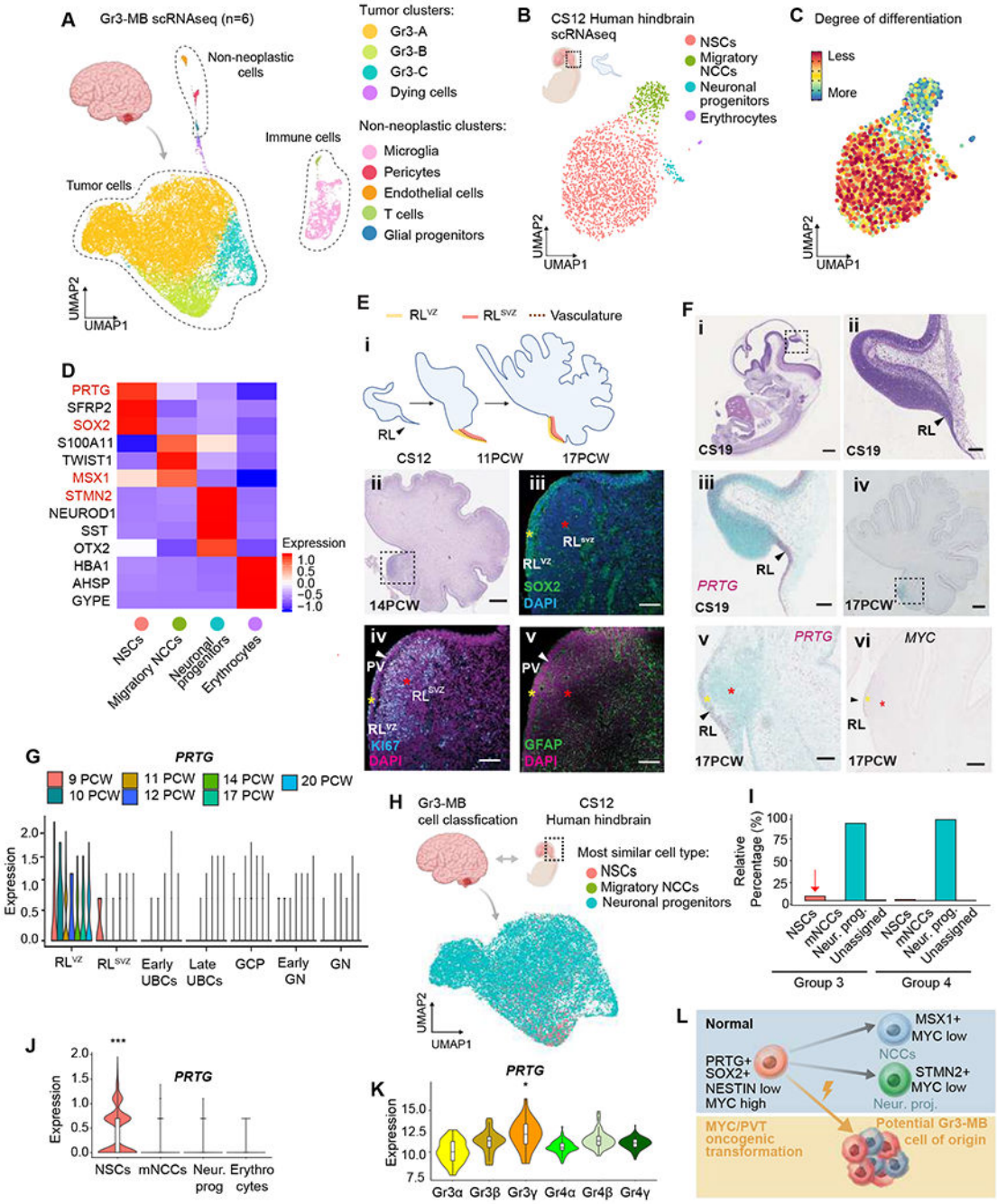

Figure 1. Apical Gr3-MB Clusters Transcriptionally Mirror CS12 *Homo Sapiens* Hind Brain Stem Cells

(**A**) Uniform manifold approximation and projection (UMAP) visualization of integrated Gr3-MB cells (n=6 tumors) demonstrates nine distinct transcriptional clusters.

(**B**) UMAP visualization of the developing *Homo sapiens* hindbrain at Carnegie stage 12 (CS12) demonstrating four distinct transcriptional clusters. NSC=neural stem cell. NCC=neural crest cells.

(**C**) CytoTRACE output of CS12 cell clusters demonstrating the extent of cellular differentiation. The NSC cluster consists predominantly of stem-like cells, whereas neural crest cells (NCC) and neuronal progenitor cells are more highly differentiated.
(**D**) Heatmap demonstrating scaled expression of key marker genes across distinct human hindbrain cell types.
(**E**) (i) Graphics illustrating sagittal sections of human hindbrain development at stages CS12, 11PCW and 17PCW. Arrowhead identifies the RL at CS12, which eventually splits into RL^{VZ} and RL^{SVZ} through 11 and 17PCW (yellow and red respectively). (ii) H&E staining of 14PCW developing cerebellum. Boxed inset denotes the nodulus containing the enfolded rhombic lip. (iii) SOX2 expression is high in the RL^{VZ}, (yellow asterisk), but diminished in the RL^{SVZ} (red asterisk). (iv) The human RL is proliferative, particularly the RL^{SVZ}, with extensive Ki67 staining. The RL^{VZ} and RL^{SVZ} are demarcated by a thin $GFAP^{+ve}$ interposed vascular plexus (arrowhead). RL^{VZ} stem cells migrate across the vascular plexus to become RL^{SVZ} progenitor cells. Scale bar= 100 μm, PV= Perivascular niche
(**F**) (i) and (ii) Mid-sagittal sections of the developing human hindbrain at CS19 stained with hematoxylin and eosin (H&E). Arrowheads point to the human rhombic lip (RL). (iii) *In Situ* hybridization demonstrates high *PRTG* RNA expression in the CS19 embryonic RL. (iv) and (v) After splitting of the rhombic lip at 17 PCW, *PRTG* expression is restricted to the RL^{VZ} (yellow asterisk). (vi) *MYC* expression is restricted to RL^{VZ} region at 17PCW, the same compartment as $PRTG^{+ve}$ and $SOX2^{+ve}$ cells, Scale bar= (i)-1mm, (ii-vi)-100μm
(**G**) Violin plot of cumulative *PRTG* RNA expression across different cell types of developing human fetal hindbrain from PCW9 to PCW20 demonstrates compartmentalized expression restricted to the RL^{VZ}. Mature cell types (UBCs, GCP, GN) lack *PRTG* expression.
(**H**) UMAP visualization of predicted cell types with tumor cells as input and CS12 hindbrain cells as reference using CHETAH package. Predicted cell types are colored and over laid on Gr3-MB UMAP embeddings.
(**I**) Comparison of predicted cell type proportions of Gr3-MB and Gr4-MB tumor cells using CS12 human hindbrain cells as reference.
(**J**) Violin plot of *PRTG* RNA expression levels across human hindbrain cells at CS12.
(**K**) Comparison of *PRTG* RNA expression across Gr3-MB and Gr4-MB patients shown by violin plot. The highest level of PRTG is detected in Gr3γ, the aggressive and worst prognosis medulloblastoma subtype.
(**L**) Proposed model for the Gr3-MB lineage of origin. $PRTG^{+ve}/SOX2^{+ve}/ MYC^{high} / Nestin^{low}$ NSCs give rise to MYC^{low} NCCs and neuronal progenitors during normal hindbrain development. $PRTG^{+ve}/SOX2^{+ve}$ cells with *MYC* amplification and/or *PVT1-MYC* translocation are arrested in a stem-like cell state, and form the apex of the Gr3-MB hierarchy.
See also figure S1 and S2

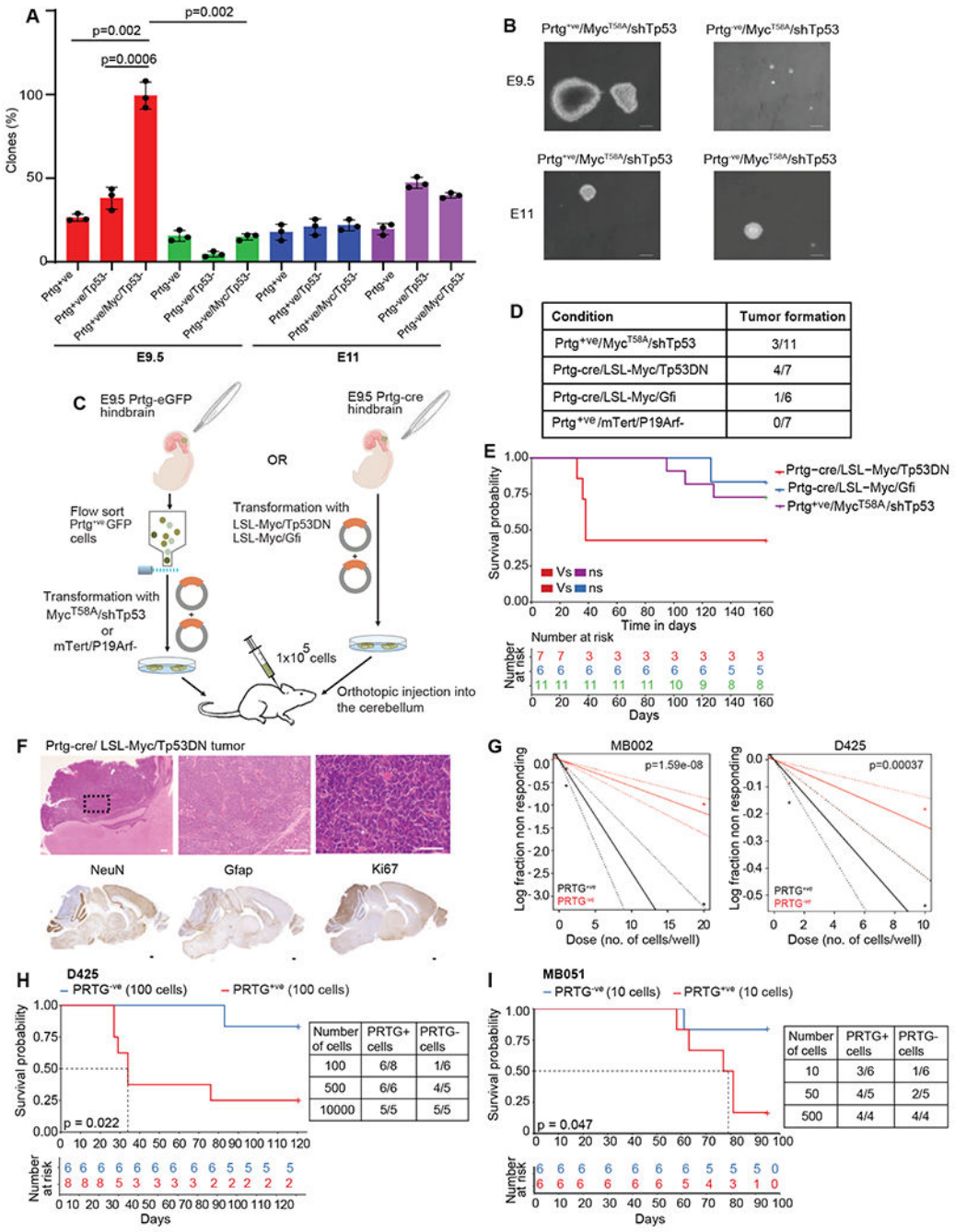

Figure 2. PRTG^{+ve} Stem Cells Initiate and Sustain Group 3 Medulloblastoma.

(**A**) Soft-agar sphere formation assay of Prtg^{+ve} versus Prtg^{-ve} controls, sorted from E9 and E11 hindbrain, and transformed by Myc over-expression (by transducing with Myc T58A), or inhibition of Tp53 (by transducing with shTp53), as labelled. The percentage of clones formed after 21 days were plotted. E9 Prtg^{+ve} hindbrain cells with high Myc and Tp53 depletion demonstrated the highest clonality compared to E9 Prtg^{-ve}, or E11 Prtg^{+ve} transformed cells. Data are represented as mean ± SEM, n=3

(**B**) Representative images of the colonies of various genotypes.

(**C**) Workflow for assessing transformation efficiency of E9.5 $Prtg^{+ve}$ hindbrain cells. $Prtg^{+ve}$ cells were either flow-sorted or isolated from E9.5 hindbrain of $Prtg^{eGFP}$ or $Prtg^{cre}$ mice. Isolated cells were transduced with Gr3-MB versus control oncogenic aberrations as labelled and grafted into the cerebella of NSG mice.

(**D**) Tumor incidence rate observed in mice injected with different combinations of driver genetic events.

(**E**) Kaplan-Meier plot of NSG mice grafted with indicated genotypes. $Prtg^{cre}$/*LSL-Myc*/*Tp53DN* (dominant negative) demonstrate the worst overall survival.

(**F**) H/E staining of mouse brains with tumors generated from E9.5 $Prtg^{cre}$ cells transformed with LSL-Myc/Tp53DN. Tumor histology recapitulates the morphology of large cell/anaplastic (LCA) medulloblastoma. The tumors are devoid of NeuN and Gfap cells, but highly proliferative. Scale bar=1mm (low), 50μm (high)

(G) PRTG positive and negative cells were flow-sorted from Gr3-MB lines MB002 and D425, and limited dilution assays were performed in 96-well plates. The number of wells without spheres were plotted using ELDA. $PRTG^{+ve}$ medulloblastoma cells demonstrate a higher degree of clonogenicity than $PRTG^{-ve}$ controls.

(H) D425 cells flow-sorted into $PRTG^{+ve}$ and $PRTG^{-ve}$ fractions were separately xenografted (100 cells) into the cerebellum of NSG mice. $PRTG^{+ve}$ cells show enhanced tumorigenic potential as compared to $PRTG^{-ve}$ cells. Table shows the fraction of mice which formed tumors, by cell count.

(I) Intracranial injection of 10 $PRTG^{+ve}$ versus $PRTG^{-ve}$ sorted cells of MB051 (Gr3 PDX line) and the survival plotted by Kaplan-Meier survival plot. $PRTG^{+ve}$ cells demonstrate increased tumorigenesis and reduced survival. Table shows the fraction of mice which formed tumors, by initiating cell count. **See also** figure S3 and S4

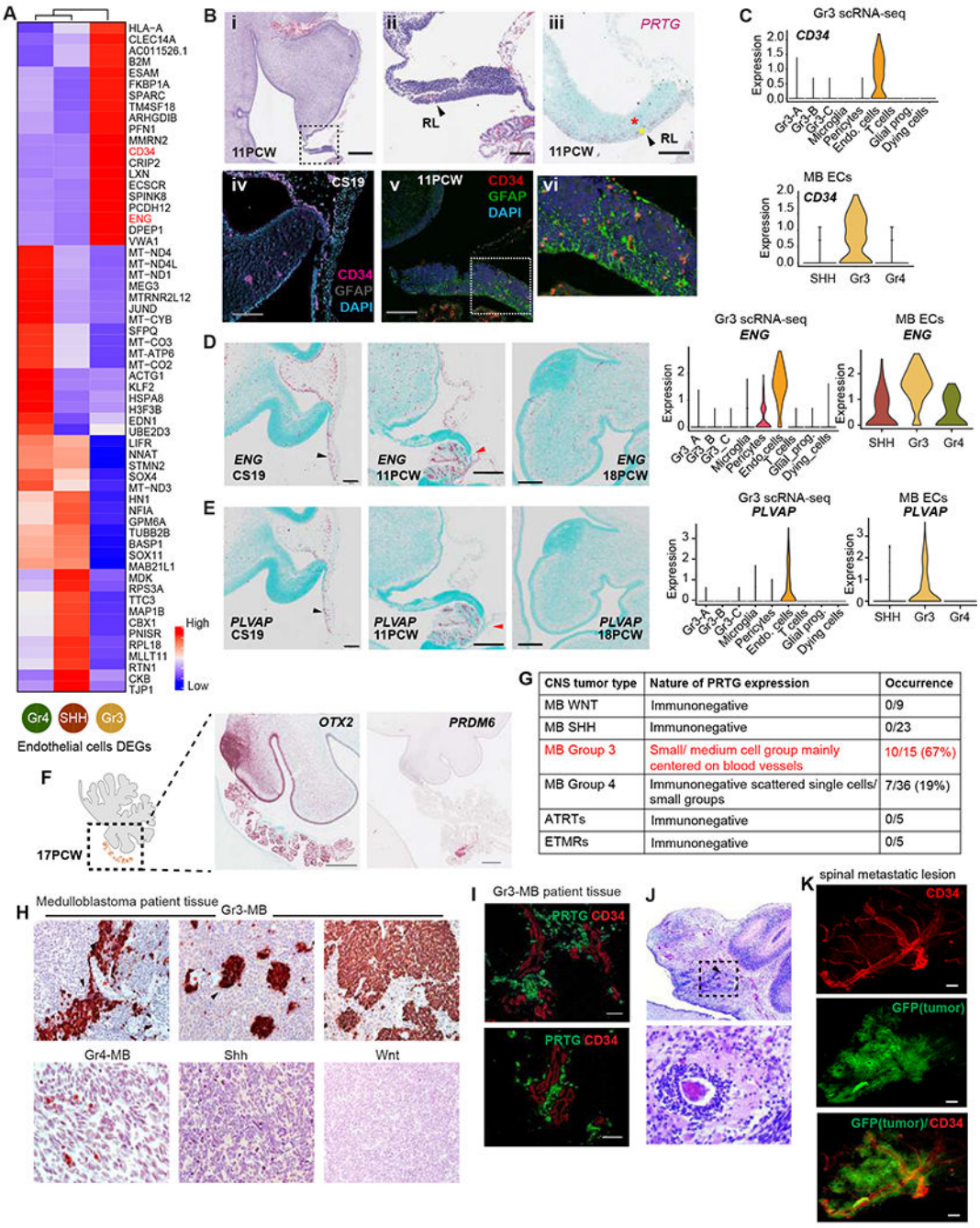

Figure 3. Normal and Malignant PRTG^{+ve} RL^{VZ} -like Cells Reside in a Perivascular Niche.

(**A**) Heatmap of scaled endothelial cluster specific gene signature from scRNA-seq showing differential expression between MB subgroups. *CD34* receptor expression is specifically enriched in ECs from Gr3-MB.

(**B**) (i) and (ii) H&E staining of 11PCW cerebellum demonstrating the structural split of the RL, and adjacent 4th ventricle choroid plexus (4V-CP). (iii) *PRTG in situ* hybridization demonstrates *PRTG* expression restricted to the RL^{VZ} region (yellow asterisk) at 11PCW. (iv) and (v) Adjacent section showing PRTG^{+ve} cells were juxtaposed to the CD34^{+ve}/

GFAP^{+ve} IVP which physically divides RL^{VZ} from the RL^{SVZ} compartment. CD34/GFAP staining shown from CS19 and 11PCW RL. (vi) Enlarged view of perivascular niche shown at 11PCW. Scale bars =(i)- 0.5mm, (ii-v)-100μm

(**C**) Expression of *CD34* is restricted to EC cluster of Gr3-MB. Comparative *CD34* expression plotted in EC clusters from SHH, Gr3-MB and Gr4-MB scRNA-seq.

(**D**) Spatial expression of Gr3-MB endothelial marker *ENG* at CS19, 11PCW (RL/CP region) and 18PCW (nodular lobe) detected by ISH. Marker shows positivity in RL vasculature and CP shown by the arrowheads (black- RL, red- CP) while reduced at 18PCW. RNA expression of *ENG* across different Gr3-MB sc-seq clusters. Predominant *ENG* expression in Gr3-MB ECs and pericytes, compared to endothelial clusters of SHH, Gr4-MB. Scale bar=200μm

(**E**) Spatial expression of *PLVAP* at CS19, 11PCW (RL/CP region) and 18PCW (nodular lobe) detected by ISH. Marker shows specific positivity in RL vasculature at CS19, and CP shown by the arrowheads while absent in 18PCW cerebellum (black- RL, red- CP). RNA expression of *PLVAP* across different Gr3-MB sc-seq clusters. Predominant *PLVAP* expression in Gr3-MB ECs, compared to endothelial clusters of SHH, Gr4-MB. Scale bar=200μm

(**F**) Cartoon of 17PCW cerebellum with adjacent 4V-CP. Spatial expression of *OTX2* at 17PCW detected by ISH showing positivity in CP and adjacent RL region. *PRDM6* expression detected by ISH showing partial positivity in CP. Scale bar=500μm

(**G**) Table showing the incidence of PRTG immunopositivity quantified by IHC in surgical biopsies of human WNT, SHH, Gr3-MB, Gr4-MB, ATRT, and ETMR patient tissues. PRTG positive clusters are unique to Gr3-MB.

(**H**) Immunohistochemical staining of human medulloblastoma surgical tissue demonstrates PRTG expression. Large clusters of PRTG^{+ve} cells (shown by arrowheads) reside in the perivascular niche (asterisks) in Gr3-MB. Gr4 MB exhibits rare, solitary PRTG^{+ve} cells, but no perivascular niche. WNT and SHH medulloblastomas are devoid of PRTG^{+ve} cells.

(**I**) Co-staining of PRTG and CD34 (HSC/endothelial marker) in Gr3-MB medulloblastoma patient tissue samples. PRTG^{+ve} cell clusters localize adjacent to the CD34^{+ve} vascular bed.

(**J**) H&E-stained mid-sagittal section of the developing third trimester human cerebellum. Arrowhead points to a persistent rhombic lip (PeRL) present in the nodulus. Higher magnification of the PeRL demonstrates clusters of small blue embryonic cells similar to the RL^{SVZ} nestled as rosettes around a conspicuous vascular structure in the cerebellar nodulus.

(**K**) Leptomeningeal metastatic medulloblastoma cells (GFP^{+ve}) inhabit a neurovascular niche marked by CD34, as demonstrated in the surgically removed leptomeninges from a mouse xenografted with an intracerebellar Med411FH PDX primary tumor. Scale bar- 50μm See also figure S5

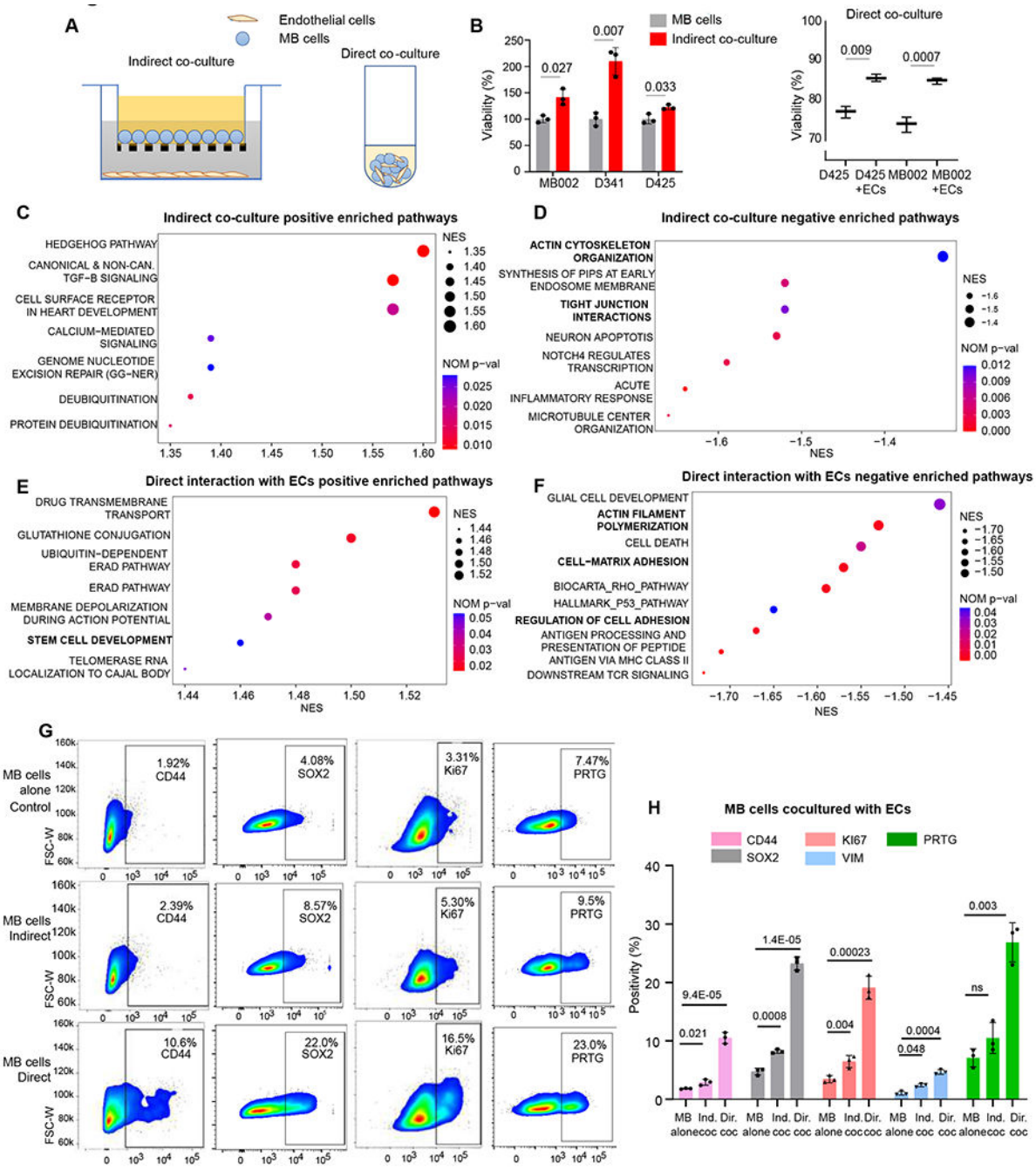

Figure 4. ECs induce malignant stem-like expression profile in Gr3-MB cells.

(**A**) Cartoon of experimental design. Gr3-MB cells and ECs were cultured either as an indirect coculture by seeding in two different chambers divided by a cell-impermeable membrane, (0.4μm) or by direct co-culture to facilitate direct EC-MB cell contact.

(**B**) Improved viability of Gr3-MB cells observed in indirect co-culture seeded with HUVEC compared to Gr3-MB cells grown alone as analysed by Alamar blue assay. Viability of control cells was considered as 100%. Viability of the direct cocultured cells with HUVEC

as measured by PI staining, followed by flow cytometry. Plot shows the percentage viability in each condition.

(**C**) Gene ontology terms for the genes positively enriched in the differentially regulated transcriptome between Gr3-MB lines grown as indirect co-culture system with ECs compared to control cells

(**D**) Gene ontology terms for the genes negatively enriched in the differentially regulated transcriptome between Gr3-MB lines grown as indirect co-culture system with ECs compared to control cells.

(**E**) Gene ontology terms for the genes positively enriched in the differential transcriptome of PDX cells proximal to vessel endothelium compared to non-interacting cells

(**F**) Gene ontology terms for the genes negatively enriched in the differential transcriptome of PDX cells proximal to vessel endothelium compared to non-interacting cells

(**G**) Enhanced expression of markers for stem-like cells/malignant markers (CD44, SOX2, PRTG) and elevated $Ki67^{high}$ cells detected in MB002 cells seeded as indirect or direct co-culture system.

(**H**) Percentage of positive cells detected for Ki67, SOX2, CD44 and PRTG in Gr3-MB cells grown alone, indirect co-culture with ECs or direct co-culture were plotted. Data are represented as mean ± SEM. n=3

See also figure S5

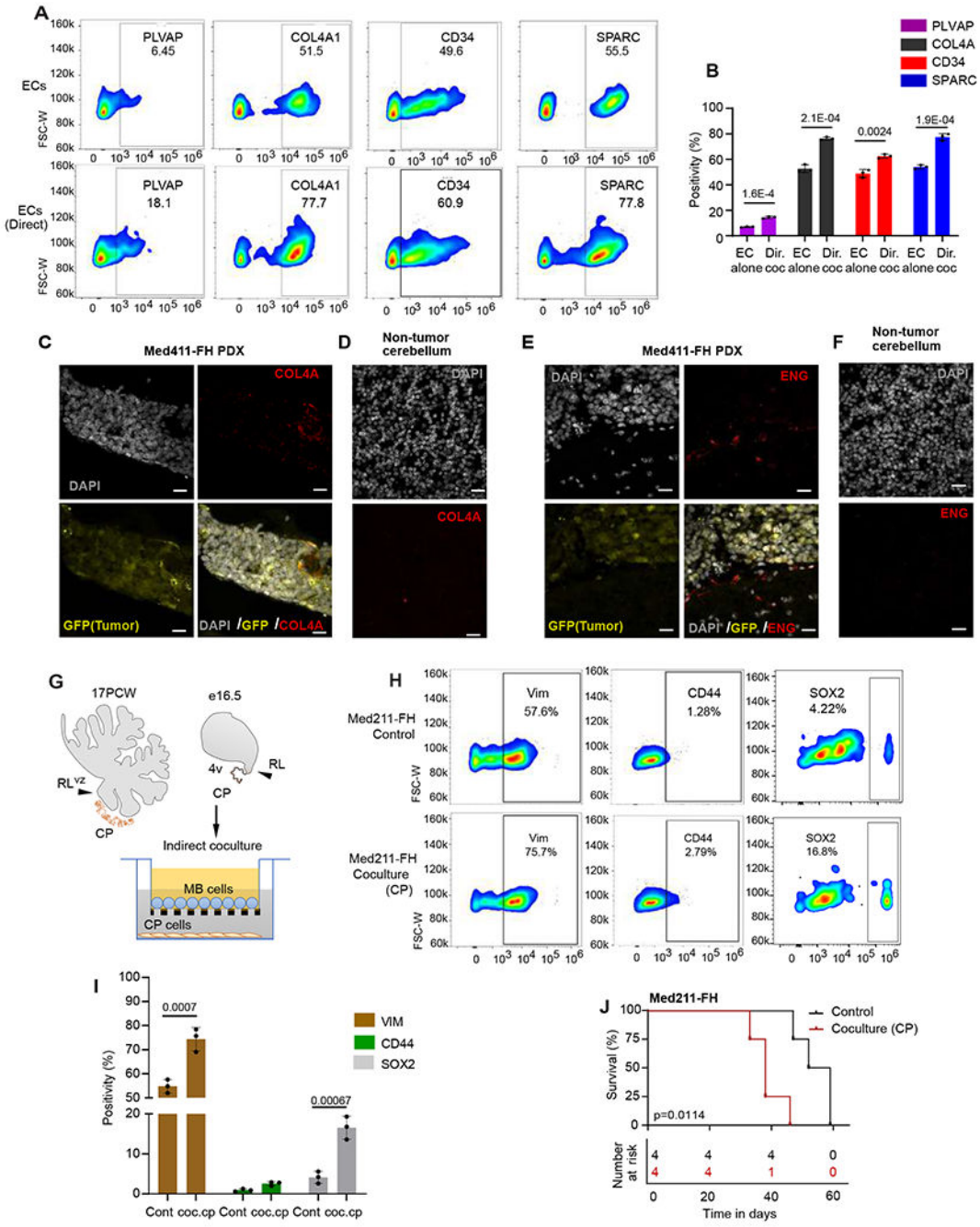

Figure 5. Gr3-MB cells Establish a Symbiotic Niche with Endothelial Cells.

(**A**) Increased expression of the Gr3-MB endothelial markers; PLVAP, COL4A, CD34 and SPARC detected in HUVEC cells grown as direct coculture with MB002 cells after 72 hrs.

(**B**) Percentage of positive cells detected for SPARC, COL4A, PLVAP and CD34 were elevated in the ECs grown as direct co-culture with MB cells compared to ECs alone. Data are represented as mean ± SEM. n=3

(**C**) High COL4A1 expressing cells are detected in the tumor-microenvironment around EGFP expressing tumor cells (Med411FH PDX tissue). Scale bar= 10μm

(**D**) Lack of expression of COL4A in the non-tumor bearing cerebellar hemisphere (Granular Layer) in the same animal (negative control) Scale bar= 10μm
(**E**) High ENG expressing cells are detected in the tumor-microenvironment cells around EGFP expressing tumor cells (Med411FH PDX tissue). Scale bar= 10μm
(**F**) Lack of expression of ENG in the non-tumor bearing cerebellar hemisphere (Granular Layer) in the same animal (negative control) Scale bar= 10μm
(**G**) Human RL^{vz} sub-structure is proximal to 4V-CP shown at 17PCW facilitating inter-compartment communication. MB cells were cocultured with E16.5 4V-CP ECs in a trans-well chamber with a 0.4μm filter to facilitate paracrine cell-cell signalling.
(**H**) MB cells cocultured with E16.5 4V-CP ECs in the lower chamber demonstrate increased positive expression of CD44, Vimentin and SOX2 compared to control MB cells.
(**I**) Equal numbers of Med211FH control cells, or Med211FH cells that were cocultured with E16.5 4V-CP ECs in the insert were orthotopically implanted into NSG mice. Mice injected with from indirect co-culture show poor survival compared to control cells.
See also figure S5

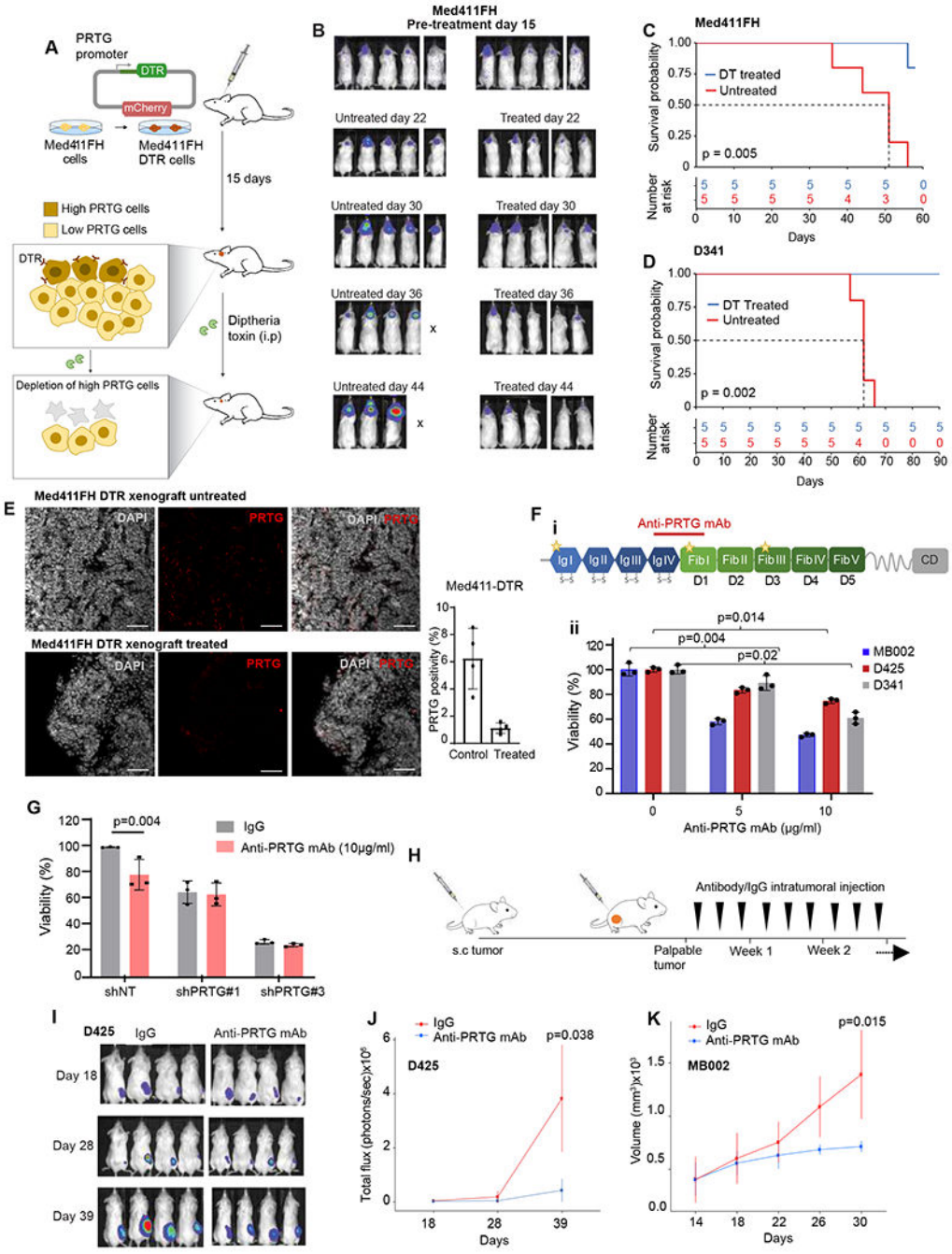

Figure 6. Ablation of PRTG^{+ve} Compartment Reduces Viability of Gr3-MB.

(**A**) Workflow for PRTG^{high} compartment depletion using the Diptheria Toxin Receptor (DTR) system. DTR was cloned downstream of the PRTG promoter (1.5kb) and transduced into the patient derived Gr3-MB line Med411FH. Post orthotopic implantation, mice were treated with intraperitoneal Diphtheria toxin thrice a week for 3 weeks.

(**B**) Reduced tumor growth in treated Med411FH PRTG-DTR mice versus untreated controls as demonstrated by bioluminescence imaging (BLI).

(**C**) Kaplan-Meier survival plot showing depletion of the $PRTG^{+ve}$ cells in Med411FH PRTG-DTR tumors by DT treatment improves survival. P value was analyzed by two-sided log-rank test.
(**D**) Kaplan-Meier survival plot of untreated and Diptheria toxin (DT) treated mice carrying D341 DTR xenograft tumors. PRTG compartment ablation prolongs survival.
(**E**) Med411FH-DTR xenografts treated with diphtheria toxin versus untreated Med411FH-DTR controls were stained for PRTG expression. DT treatment successfully depleted the $PRTG^{+ve}$ compartment in treated animals. Data are represented as mean ± SEM.
(**F**) (i) Cartoon depicting the domains of the transmembrane PRTG protein. The extracellular domain includes Ig-like (Ig I-IV) and fibronectin domains (Fib I-V). Stars indicate glycosylation sites, while disulfide bridges are depicted by links. The target site for the anti-PRTG mAb is indicated. (ii) Incubation of Gr3-MB cells with control IgG or anti-PRTG mAb for 7 days reduced the viability of anti-PRTG treated cells as measured by Alamar blue dye.
(**G**) Viability of shNT and shPRTG MB002 cells was assessed after treating with IgG or anti-PRTG mAb (10μg/ml). shPRTG cells fail to respond to mAb treatment. Viability was measured by Alamar Blue dye and shNT condition was considered as 100%. n=3
(**H**) Experimental plan for *in vivo* anti-PRTG mAb treatment. Gr3-MB lines were grafted subcutaneously (s.c) into NSG mice, which were treated with anti-PRTG mAb (100μg) by intra-tumoral injection 3 times a week after palpable flank tumor formation.
(**I**) Representative BLI images of the D425 flank tumors showing reduced tumor progression after Anti-PRTG mAb therapy as compared to IgG treated controls.
(**J**) Total luciferase flux quantification over time of IgG versus anti-PRTG treated tumors demonstrates the survival advantage of anti-PRTG mAb treatment. Data are represented as mean ± SEM. n=4
(**K**) Anti-PRTG mAb treated MB002 flank tumors show reduced volume compared to control animals treated with IgG. Data are represented as mean ± SEM, n=4

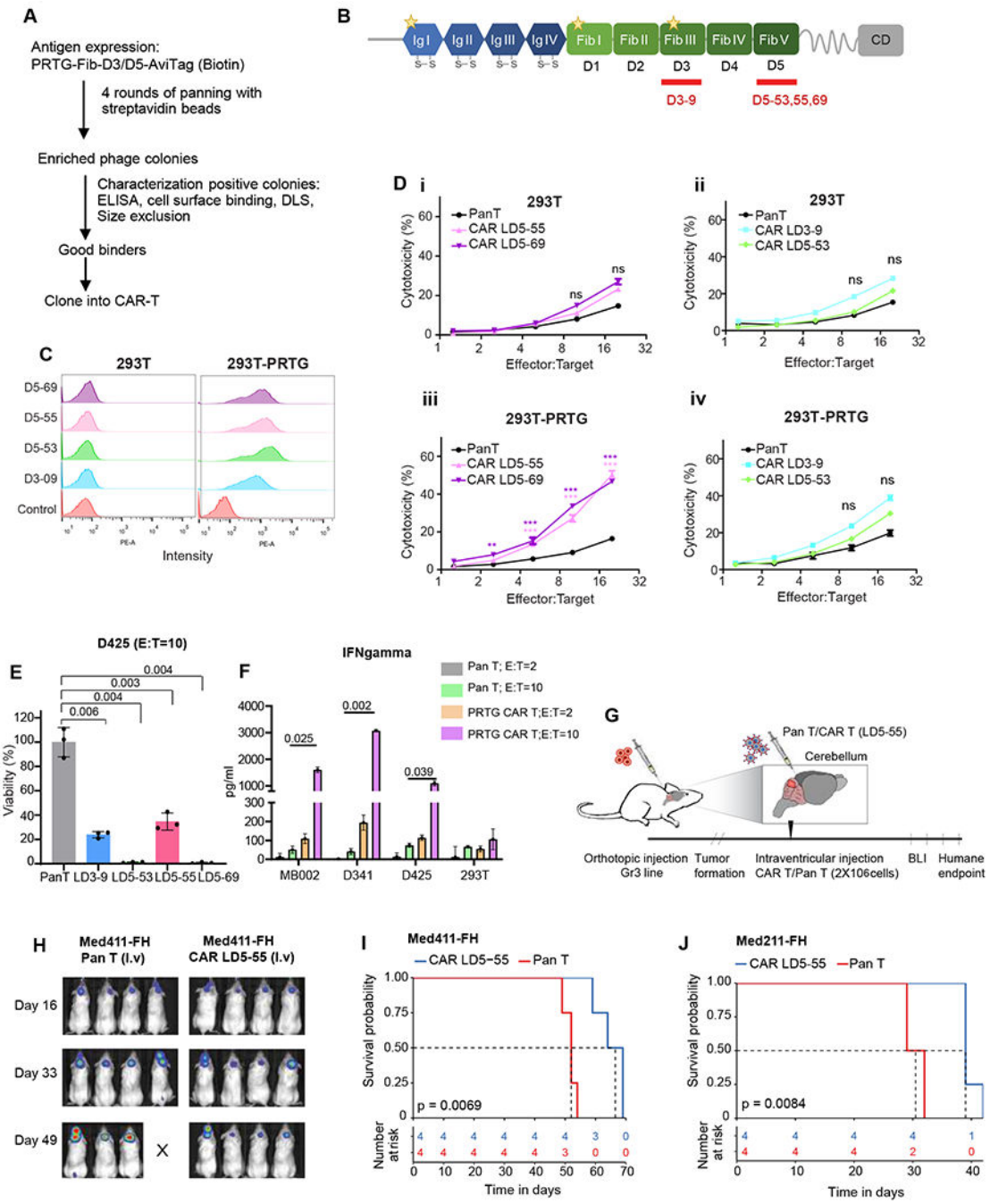

Figure 7. Targeted Depletion of the PRTG^{+ve} Compartment by CAR T-cells Impairs Medulloblastoma.

(**A**) Overview of the phage panning approach to select human antibody heavy chain VH binders for PRTG. The PRTG domains were expressed in Expi293 cells and biotin labeled. Four rounds of panning were performed to enrich anti-PRTG specific colonies. After characterization, the best binders were chosen for CAR T-cell development.

(**B**) Cartoon depicting the target binding sites for CAR T-cells (D3-9, D5-53, 55, 69) at PRTG are illustrated by red bars.

(**C**) Binder detection efficiency was analyzed by flow cytometry. Binding intensities of D3-9, D5-53, D5-55 and D5-69 were compared between 293T cells over expressing PRTG and control cells.

(**D**) The cytotoxicity of anti-PRTG CAR T-cells against 293T and 293T-PRTG cells. As a negative control, anti-PRTG CAR T-cells (VH55, VH69, LD3-9, LD5-53) were co-cultured with 293T cells. Anti-PRTG CAR T-cells were co-cultured with 293T-PRTG for 48 hours. Supernatant LDH was used to detect cytotoxicity. Cytotoxicity (%) was calculated at effector: target ratios of 1.25:1, 2.5:1, 5:1, 10:1 and 20:1 and compared with the Pan T group. Data are represented as mean ± SEM, n=3

(**E**) The inhibition (killing) of D425 cells by anti-PRTG CAR T-cells. Anti-PRTG CAR-T cells (effector cells) were co-cultured with D425 (target cells) at 10:1. D425 cells were stained with trypan blue. Live cells in anti-PRTG CAR T-cell groups were compared to control Pan T-cells. Data are represented as mean ± SEM, n=3

(**F**) MB and HEK293T cell lines were co-cultured with Pan T or PRTG CAR T (LD5-55) cells. Supernatants were analyzed for IFN-gamma secretion by Enzyme-Linked Immunosorbent Assay. Cytokine release was confirmed in LD5-55 treated MB cell condition at E:T=10

(**G**) Experimental plan. Gr3-MB cells were xenografted into the cerebellum of NSG mice. Once the tumor formation was confirmed by BLI, anti-PRTG CAR T- cells (LD5-55), or non-transduced Pan T-cells were delivered by lateral ventricle injection. Tumor progression was monitored by BLI.

(**H**) Representative images from the BLI of Pan T or anti-PRTG CAR T (LD5-55) injected mice carrying Med411FH xenografts showing the reduction in tumor growth in mice treated with anti-PRTG CAR T-cell treatment.

(**I**) and (**J**) Kaplan-Meier plot showing prolonged survival of anti-PRTG CAR T-cell treated Med411FH and Med211FH xenograft mice. P value calculated by log rank. Xenografts were treated with anti-PRTG CAR T (LD5-55 clone) by intraventricular injections.

See also figure S6 and S7